Total Pages - ii and 49

HEAT TRANSFER AND PRESSURE DISTRIBUTION ON A TWO-DIMENSIONAL BLUNTED ASYMMETRIC BODY.

TECHNICAL REPT. No. 204

by Mitchell Seidman

CONTRACT NO. AF 33(616)-6692

Prepared For

Commander
Wright Air Development Center
Air Research and Development Command
Wright-Patterson Air Force Base, Ohio

Prepared By

General Applied Science Laboratories, Inc.
Merrick and Stewart Avenues
Westbury, L.I., New York

December 1960

Copy ( ) of ( )

Approved by: _____

Antonio Ferri
Technical Director

TABLE OF CONTENTS

HEAT TRANSFER AND PRESSURE DISTRIBUTION ON A TWO-DIMENSIONAL BLUNTED ASYMMETRIC BODY

By Mitchell Seidman

I SUMMARY

Heat transfer and pressure distributions have been obtained on a two-dimensional asymmetric body designed to reduce heat transfer rates at the stagnation point. Theoretical and experimental pressure distributions indicate a large reduction in velocity gradients at the stagnation point. Experimental heat transfer results at the high angles of attack ($\alpha = 30^{\circ}$) indicate a 15 - 20% reduction from the two-dimensional stagnation point heat transfer. Further investigation at the higher angles of attack is desirable in order to fully evaluate the capabilities of such shapes.

II INTRODUCTION

Experimental pressure and heat transfer distributions on an asymmetric, two-dimensional body (Figure 1) are presented. This body shape was designed to determine if lower heat transfer rates can be obtained in the region of the stagnation point. Tests were conducted in Tunnel B-2 of the Arnold Engineering Development Center Gas Dynamics Facility. The test Mach number was 8.08 and the Reynolds Number per foot was 2×10^6. Stagnation pressure and temperature were approximately 480 psia and 1350°R respectively. Tests were conducted for angles of attack from -15° to 30°.

This report is presented as a part of the requirements of Air Force Contract No. AF 33(616)-6692, dated 25 May, 1959.

III DISCUSSION OF RESULTS

Pressure and heat transfer distributions were obtained for the full range of angle of attack, -15° to $+30^{\circ}$. The pressure distribution is presented as P/P_{se} versus S/R_o where P is the pressure of the model tap at a distance S from the nose, and P_{se} is the stagnation pressure behind the normal shock. The nose radius of the model, R_o, is 1/2 inch. The distance S/R_o is defined as positive on the lower surface and negative on the upper surface. Pressure tap and thermocouple locations are given in Table 1.

Heat transfer data are plotted as the ratio of the Nusselt Number based on stagnation conditions divided by the square root of the modified Reynolds Number, $Nu/\sqrt{\tilde{Re}}$, versus S/R_o where:

$$Nu = \frac{\dot{q}_w C_{P_{se}} R_o}{k_{se}(h_{se}-h_w)} \qquad (1)$$

$$\tilde{Re} = (\phi_{se})^{1/2} Re \qquad (2)$$

$$Re = \frac{\rho_{se}\sqrt{h_{se}}\, R_o}{\mu_{se}} \qquad (3)$$

$$\phi_{se} = \frac{P_{se}}{\rho_{se} h_{se}} \qquad (4)$$

All symbols are defined in Table II.

A theoretical analysis was made for the heat transfer distribution at 0°, 15° and 30° angles of attack. The results of Reference 1 were employed to determine the heat transfer at the wall, $\dot{q}_w$, necessary for computing the Nusselt Number. This quantity, $\dot{q}_w$, and thus the heat transfer, $Nu/\sqrt{Re}$, is a function of the pressure distribution, P/P_{se}. The heat transfer distribution was computed employing the method of Reference 1 for the experimental pressure distribution and the Newtonian- Prandtl-Meyer pressure distribution. These pressure distributions are shown in Figures 2, 3 and 4 and the corresponding heat transfer in Figures 5 through 10.

An additional investigation was made at 15° angle of attack. A previous report (Reference 2) has presented a method for computing the pressure distribution in the subsonic regime of an asymmetric body. The results of this analysis were found to agree quite well with experimental data as shown in Figure 3. Using this theoretical pressure distribution up to the sonic points and the experimental data for the rest of the body, a heat transfer analysis was conducted. Stagnation point heat transfer showed a 40% reduction from the two-dimensional Newtonian value. The heat transfer based on this pressure distribution is shown in Figures 7 and 8.

The location of the stagnation point as determined by the experimental pressure distribution and by the theoretical pressure distribution of Reference 2 is at $S/R_o = 0.52$ for $\alpha = 15^{\circ}$. The experimental heat transfer, the heat transfer calculated from the experimental pressure

distribution and the pressure distribution from Reference 2 all indicate a maximum heating rate at stations before the pressure field stagnation point. This shift in the maximum heat transfer may be due to the steeper velocity (pressure) gradients on the portion of the nose surface above the stagnation point.

IV CONCLUSIONS

The experimental heat transfer and pressure distributions on a two-dimensional, blunt, asymmetric body have been presented. The theoretical pressure analysis shows that large reductions in heat transfer can be obtained. The results of the heat transfer tests do not indicate this large reduction because of the large scatter and the accuracy of the instrumentation. There are also conduction errors present which have been estimated to be of the order of 25% for the 5-second readings at $\alpha = 0^{\circ}$.

The results for $\alpha = 15^{\circ}$ indicate that although the stagnation point heat transfer is reduced, the maximum heat transfer has been shifted and there still exists a point on the body with heat transfer characteristics approximately the same as found in a symmetrical two-dimensional body.

The best results for heat transfer reduction occur at $\alpha = 30^{\circ}$ where even with conduction corrections included, a 15 - 20% reduction is attained. Further experimental investigation at this and possibly higher angles of attack is desirable in order to explore the complete range of usefulness of such asymmetric bodies.

REFERENCES

1. Lees, L., Laminar Heat Transfer Over Blunt-Nosed Bodies at Hypersonic Flight Speeds; Jet Propulsion, April, 1956.

2. Vaglio-Laurin, R., Supersonic Flow About Two-Dimensional Asymmetric Blunt Bodies, General Applied Science Laboratories, Inc. Technical Report No. 178, July, 1960.

TABLE I

TABULATION OF (S/R_o) FOR PRESSURE TAP AND THERMOCOUPLE LOCATIONS FOR MODEL II C

R_o = 0.5"

Upper Surface		Lower Surface	
Tap/TC	S/R_o	Tap/TC	S/R_o
1	-.1745	0	.0
3	-.3490	2	.1745
5	-.5235	4	.3490
7	-.6980	6	.5235
9	-.8725	8	.6980
11	-1.0470	10	1.7505
13	-2.2215	12	2.7505
15	-3.2215	14	3.7505
17	-4.2215	16	4.7500
19	-5.2215	18	5.7500
21	-7.964	20	8.9814
23	-10.964	22	11.9814
25	-13.964	24	14.9814
27	-16.964	26	17.9814
		28	1.2505
		30	2.2505
		32	3.2505

TABLE II - SYMBOLS

$C_{P_{se}}$	stagnation specific heat at constant pressure
h_{se}	stagnation enthalpy
h_w	wall enthalpy
k_{se}	stagnation thermal conductivity
Nu	Nusselt Number (Equation 1)
$\dot{q}_w$	local heat transfer rate at wall
P	pressure
P_{se}	stagnation pressure
Re	Reynolds Number (Equation3)
$\tilde{Re}$	defined by Equation (2)
R_o	nose radius
S	distance along body surface, measured from nose axis
α	angle of attack
ρ_{se}	stagnation density
μ_{se}	stagnation viscosity
ϕ_{se}	defined by Equation (4)

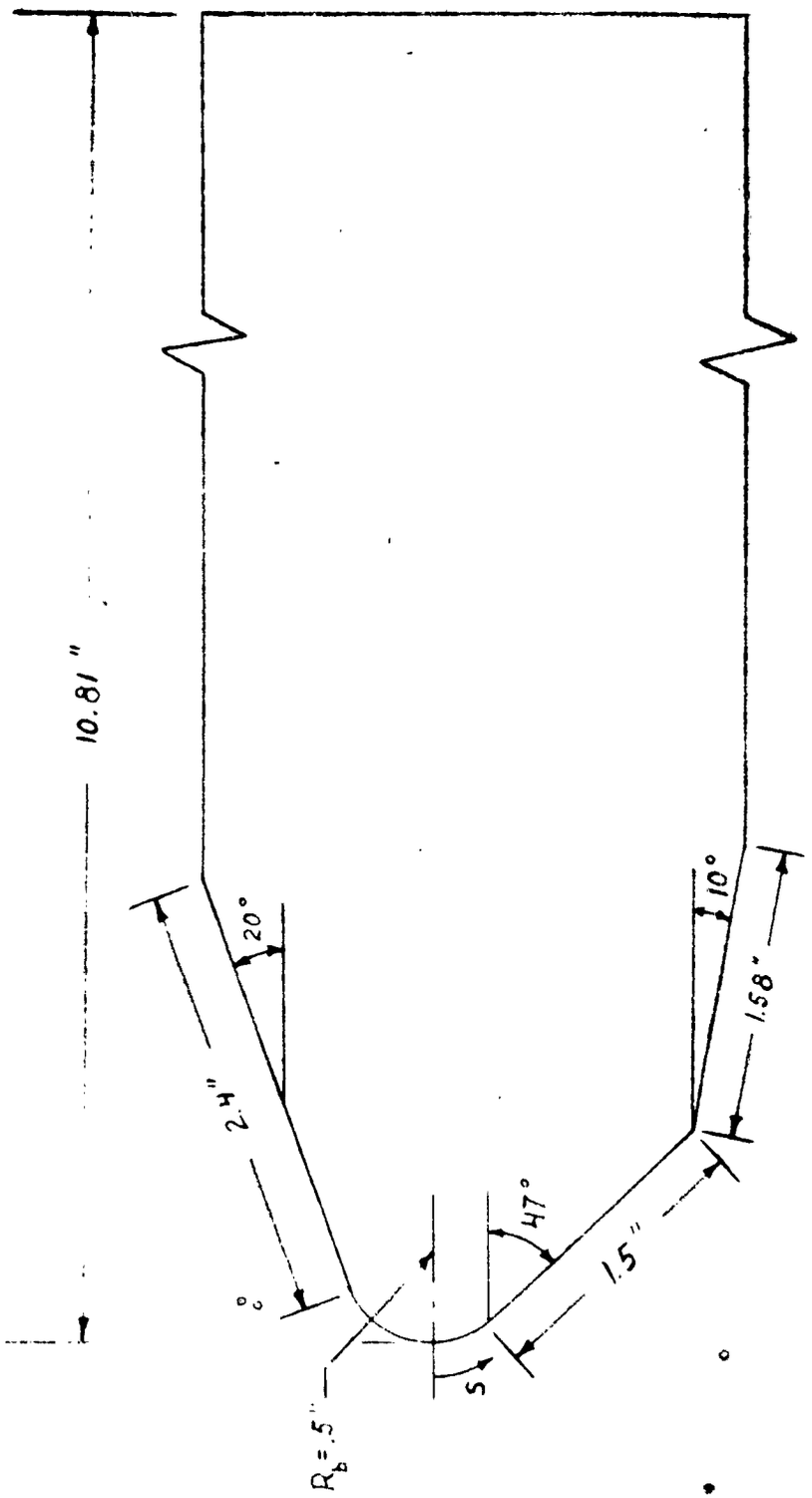

Figure 1. Scale Drawing of the Two-Dimensional, Blunt, Asymmetric Body.

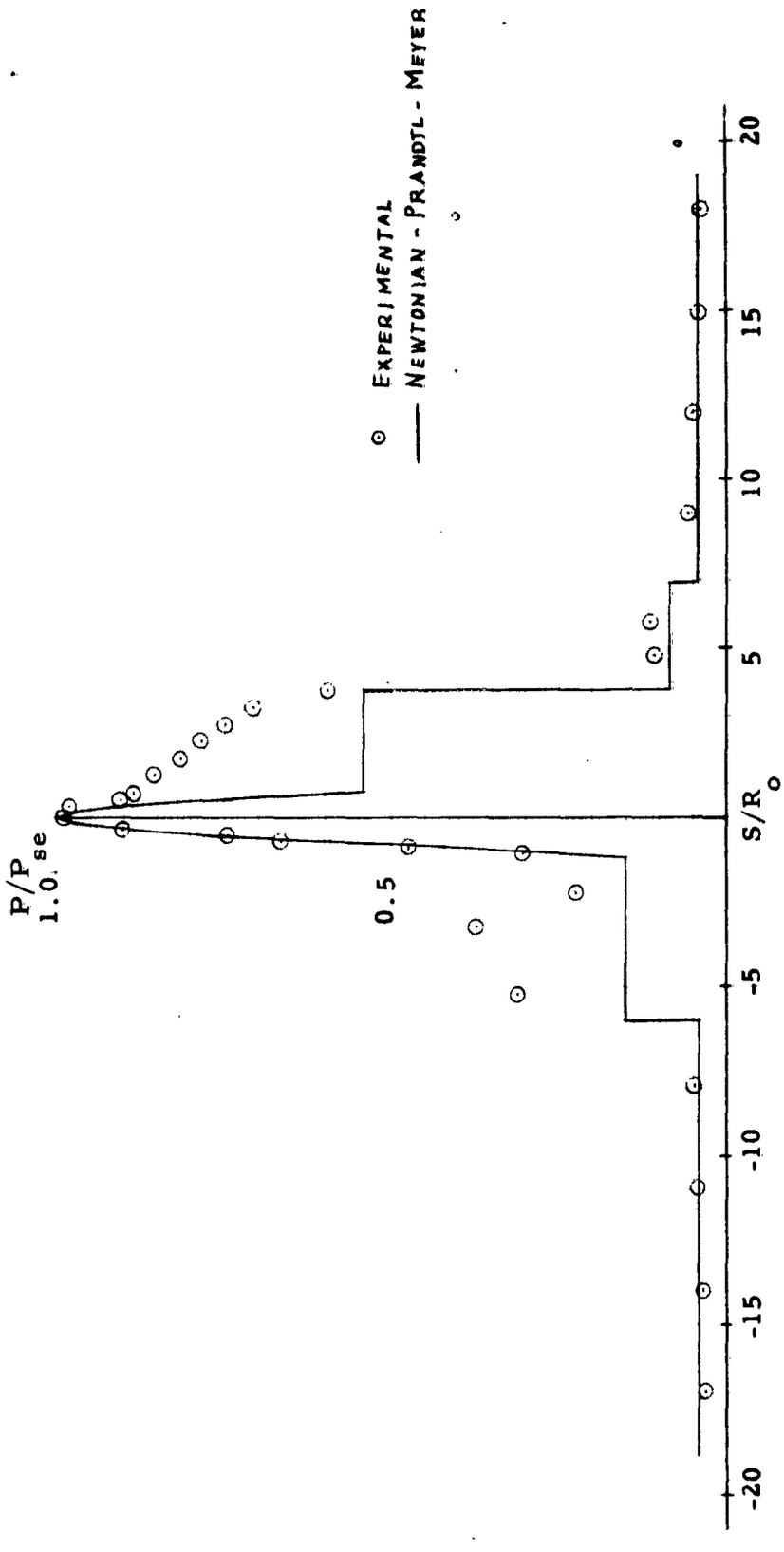

Figure 2. Experimental Pressure Distribution on Two-Dimensional, Asymmetric, Blunt Body at Mach 8.08, $\alpha = 0^{\circ}$.

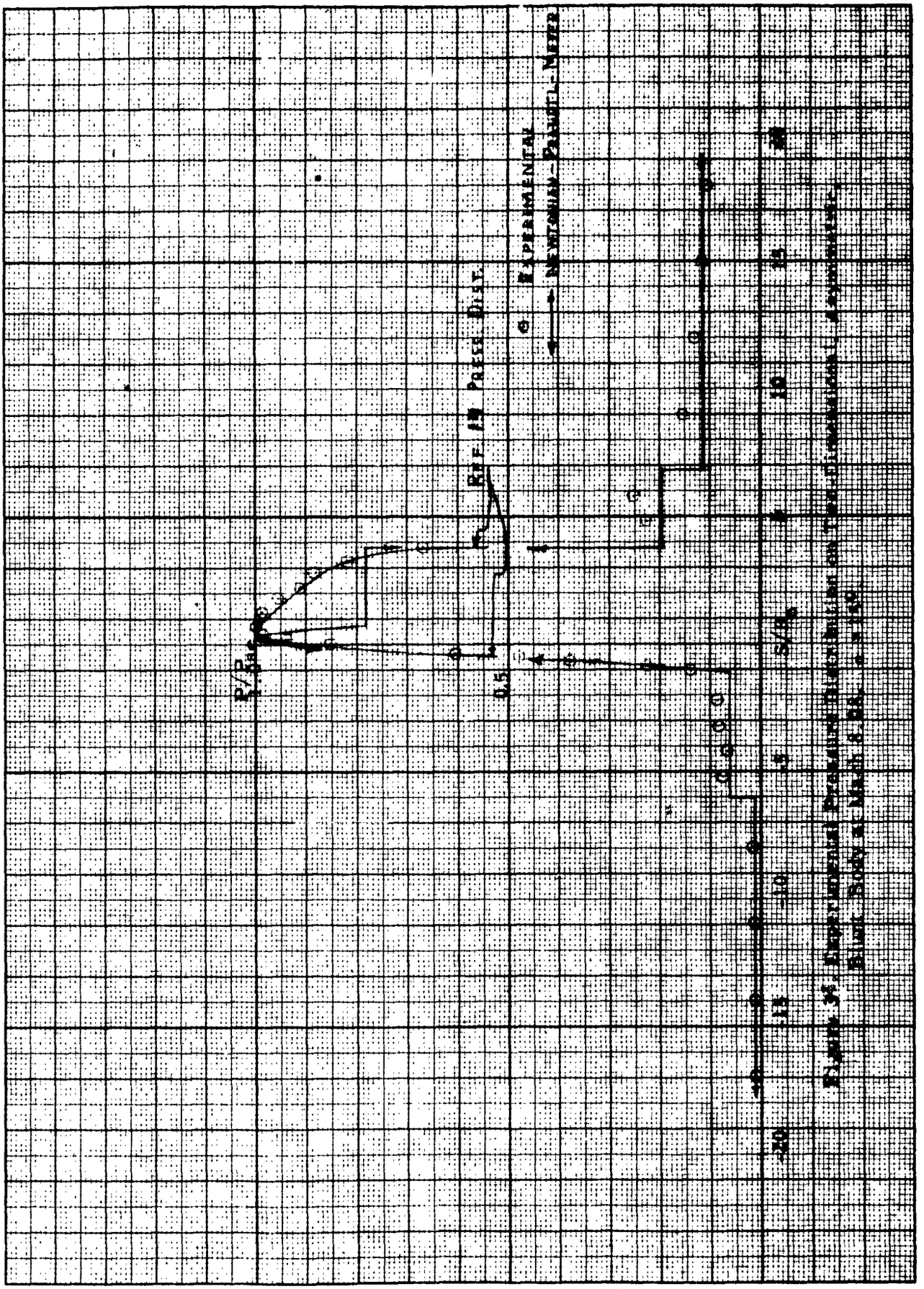

Figure 35. Experimental Pressure Distribution on Two-dimensional Asymmetric Blunt Body at Mach 8.86, $\alpha = 15°$

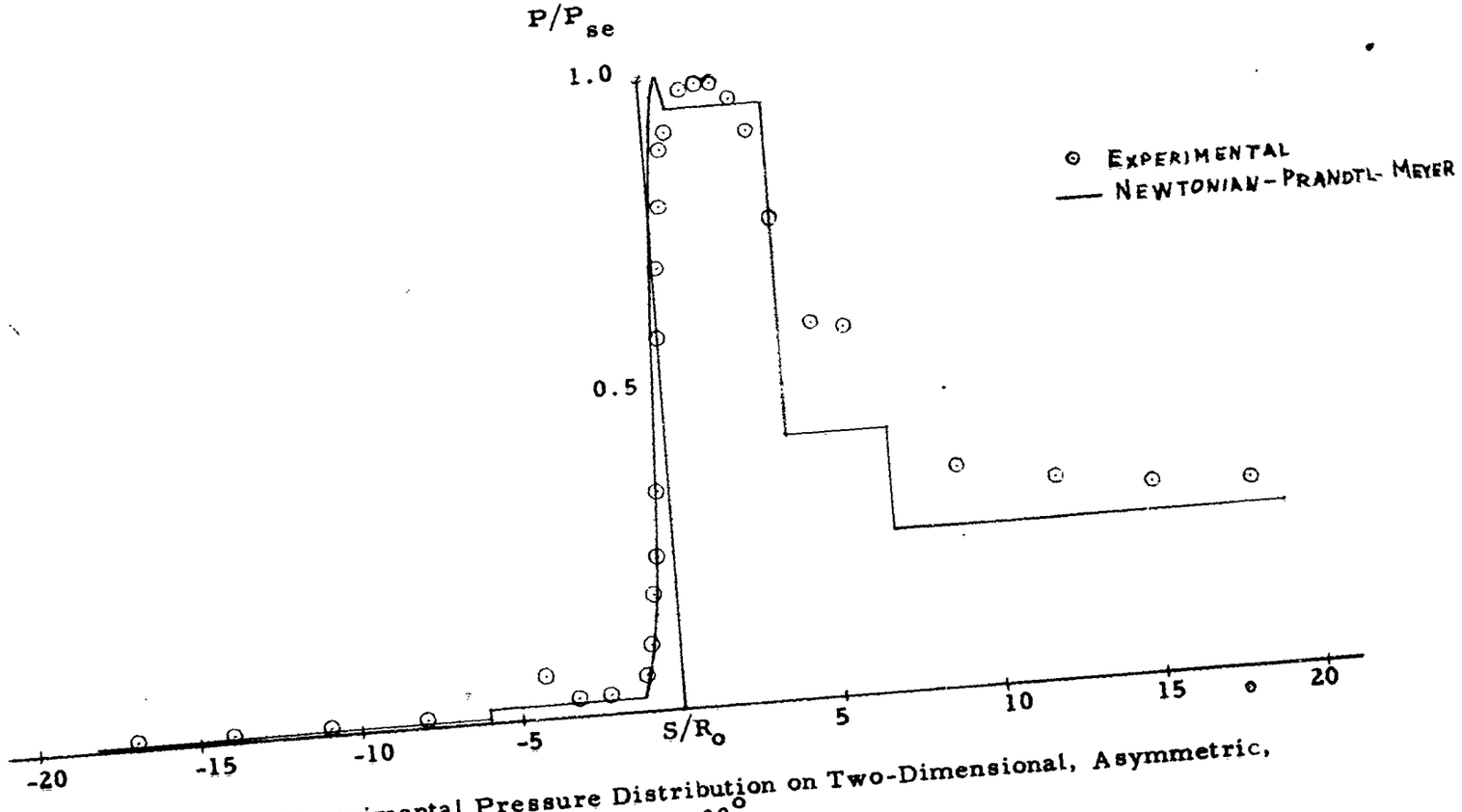

Figure 4. Experimental Pressure Distribution on Two-Dimensional, Asymmetric, Blunt Body at Mach 8.08, $\alpha = 30^{\circ}$.

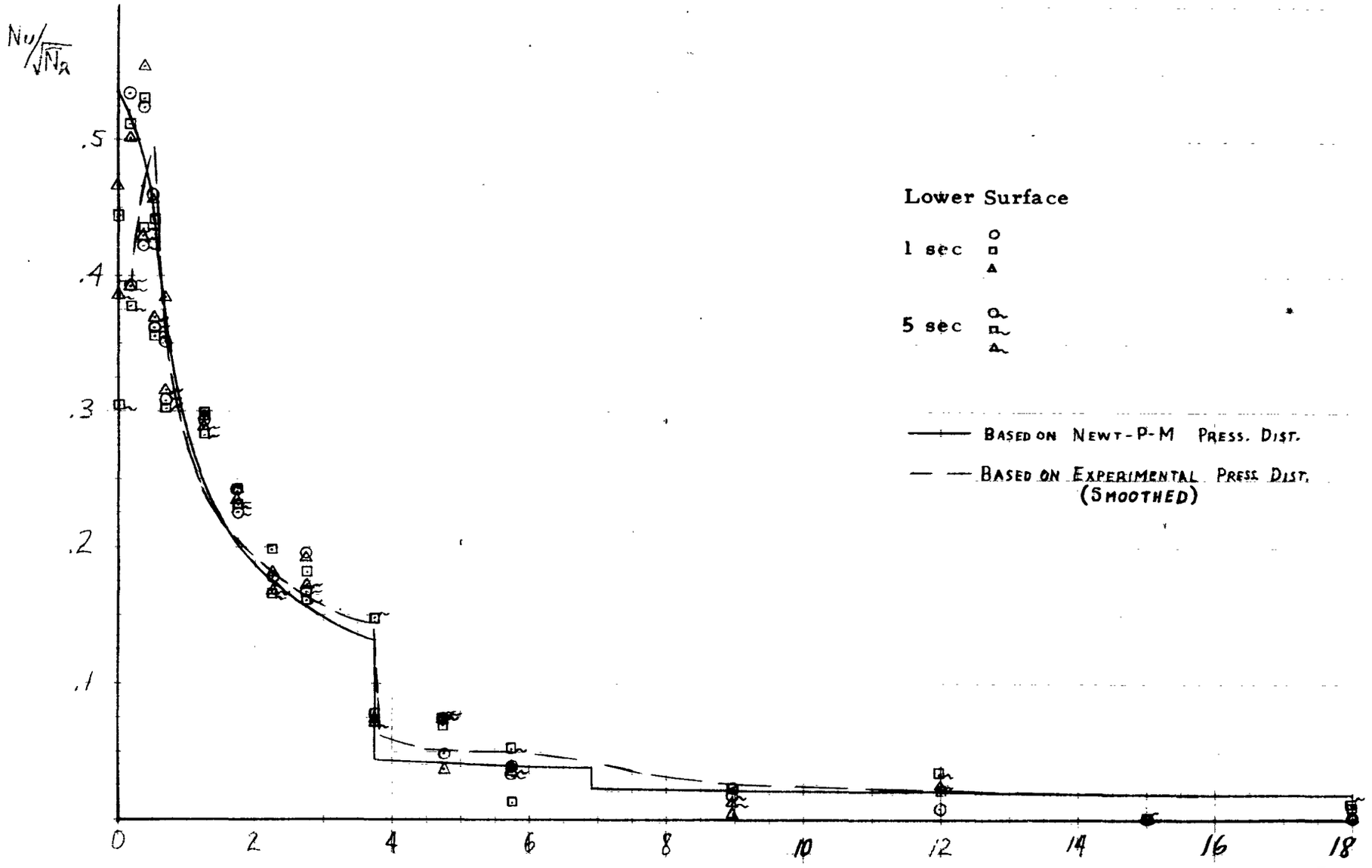

Figure 5. Experimental Heat Transfer Distribution on Two-Dimensional, Asymmetric, Blunt Body at Mach 8.08, $\alpha = 0$.

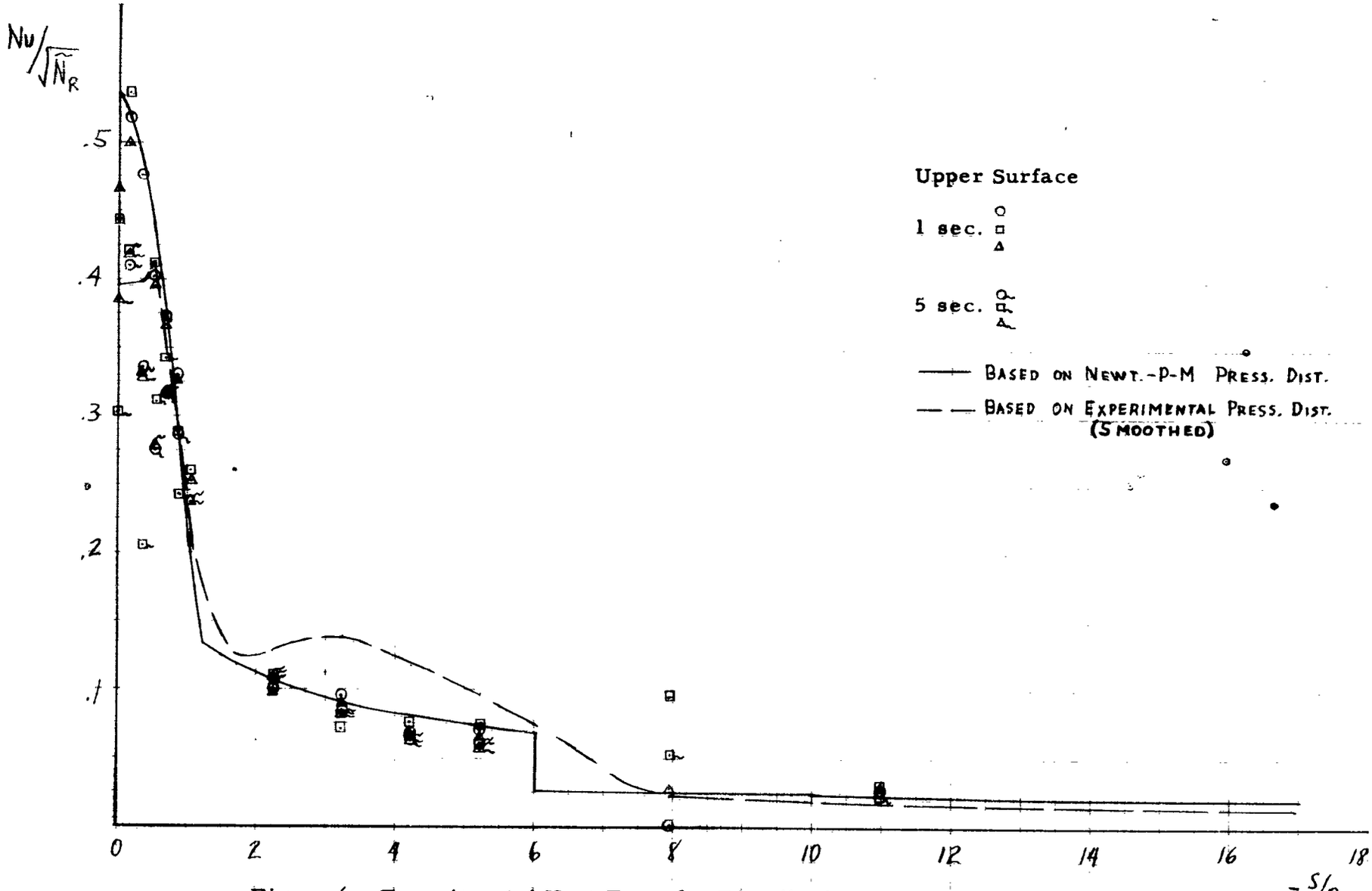

Figure 6. Experimental Heat Transfer Distribution on Two-Dimensional, Asymmetric, Blunt Body at Mach 8.08, $\alpha = 0^{\circ}$.

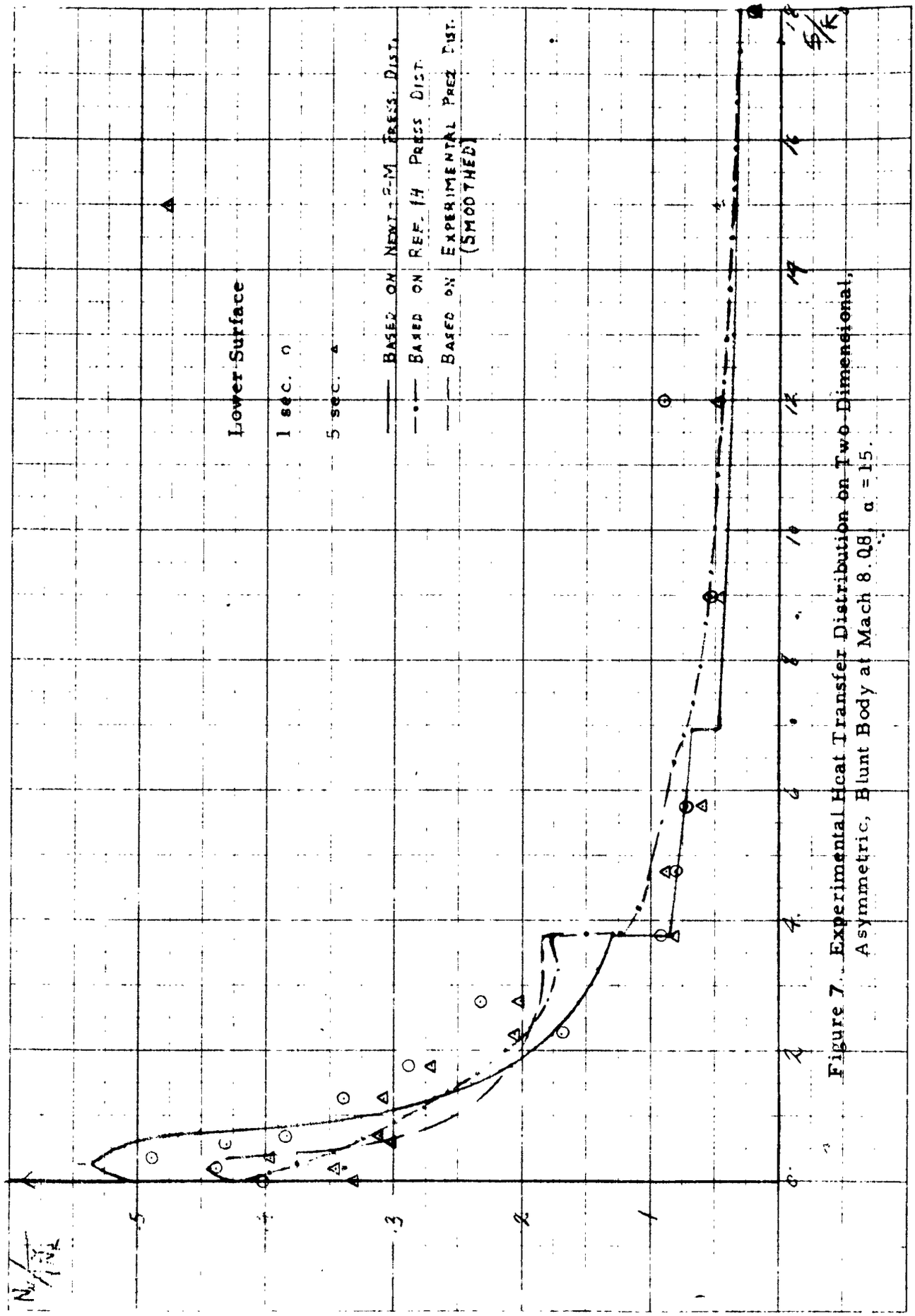

Figure 7. Experimental Heat Transfer Distribution on Two Dimensional, Asymmetric, Blunt Body at Mach 8.08, $\alpha = 15°$.

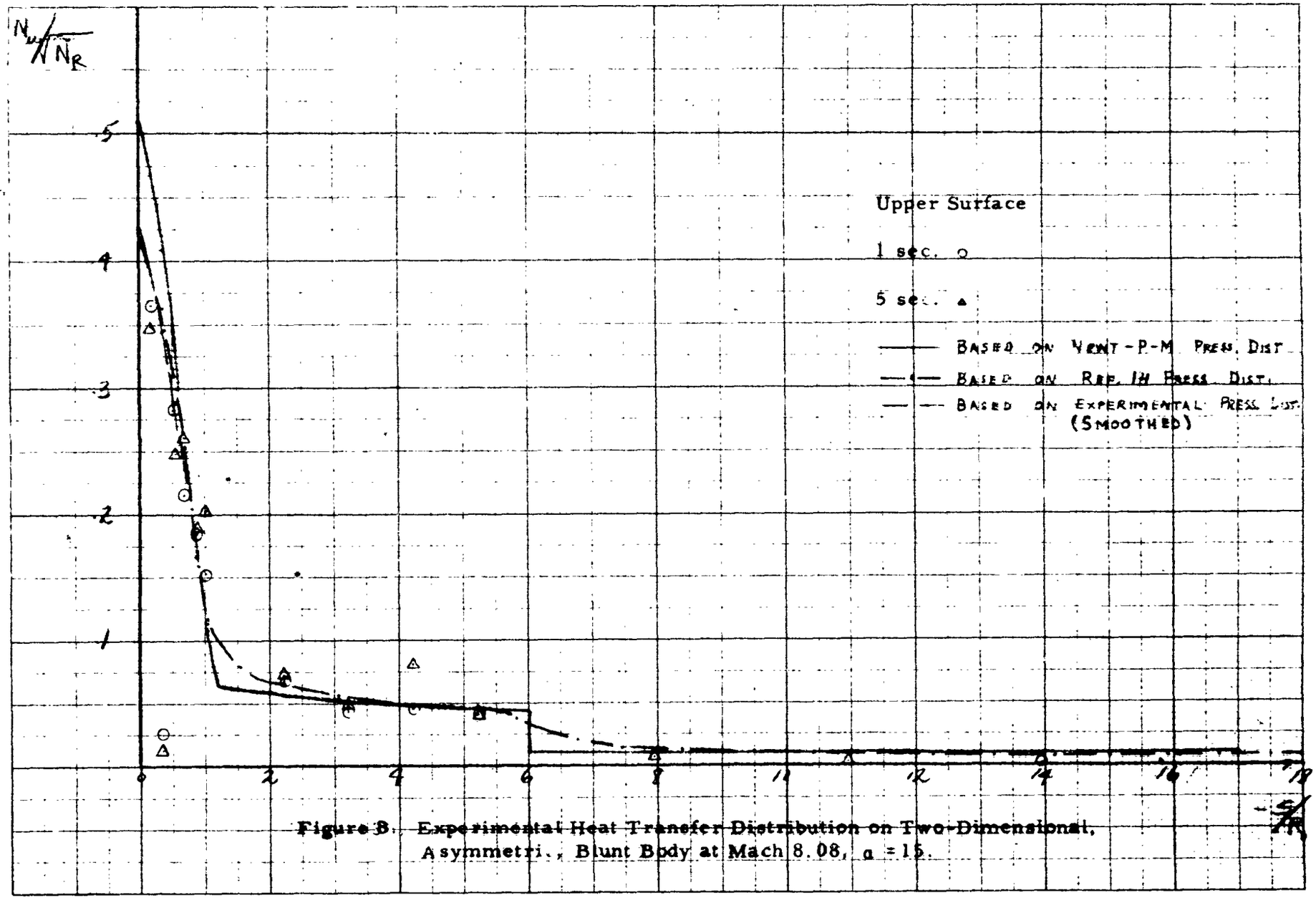

Figure 8. Experimental Heat Transfer Distribution on Two-Dimensional, Asymmetri., Blunt Body at Mach 8.08, α = 15.

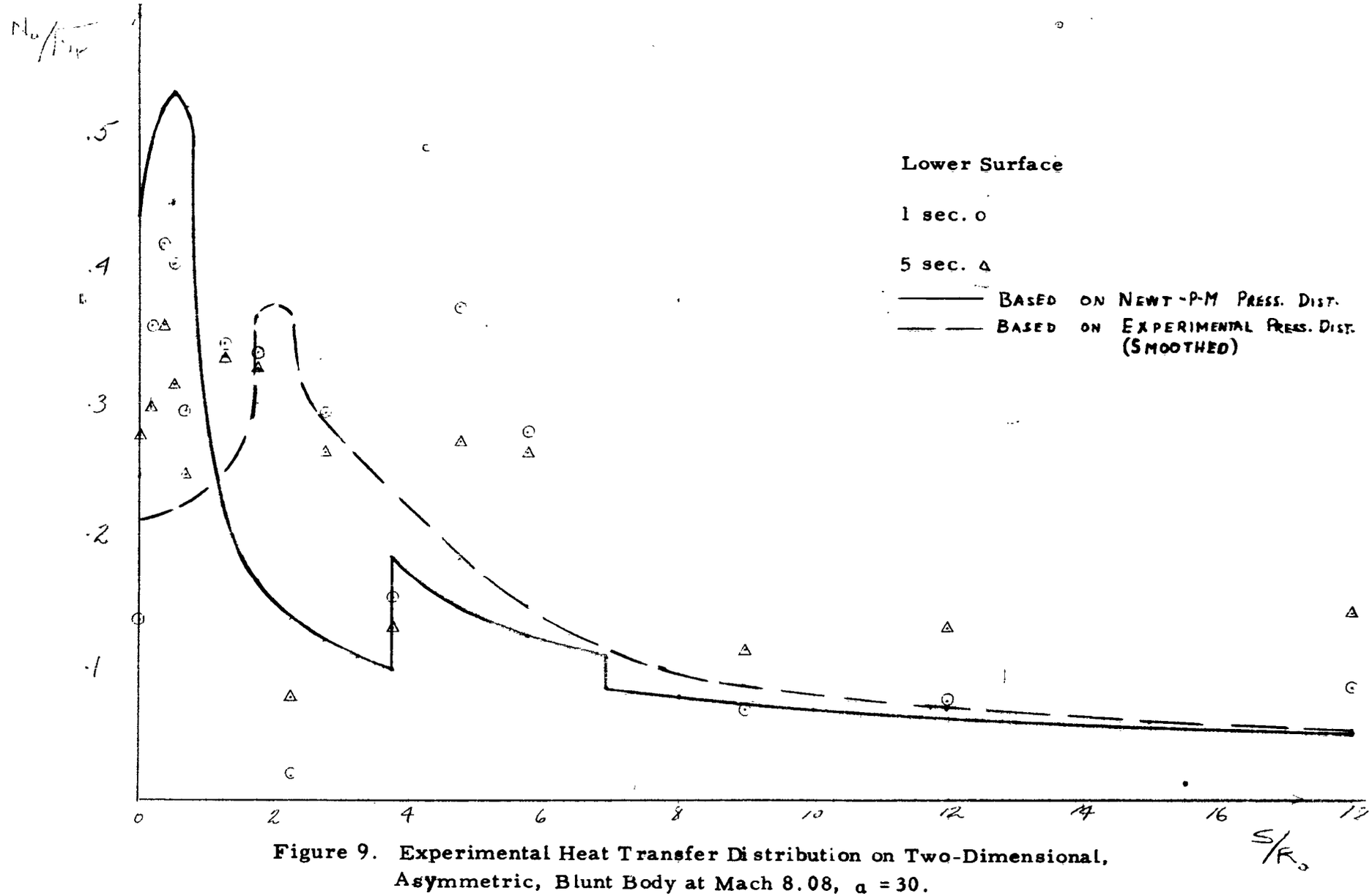

Figure 9. Experimental Heat Transfer Distribution on Two-Dimensional, Asymmetric, Blunt Body at Mach 8.08, $\alpha = 30$.

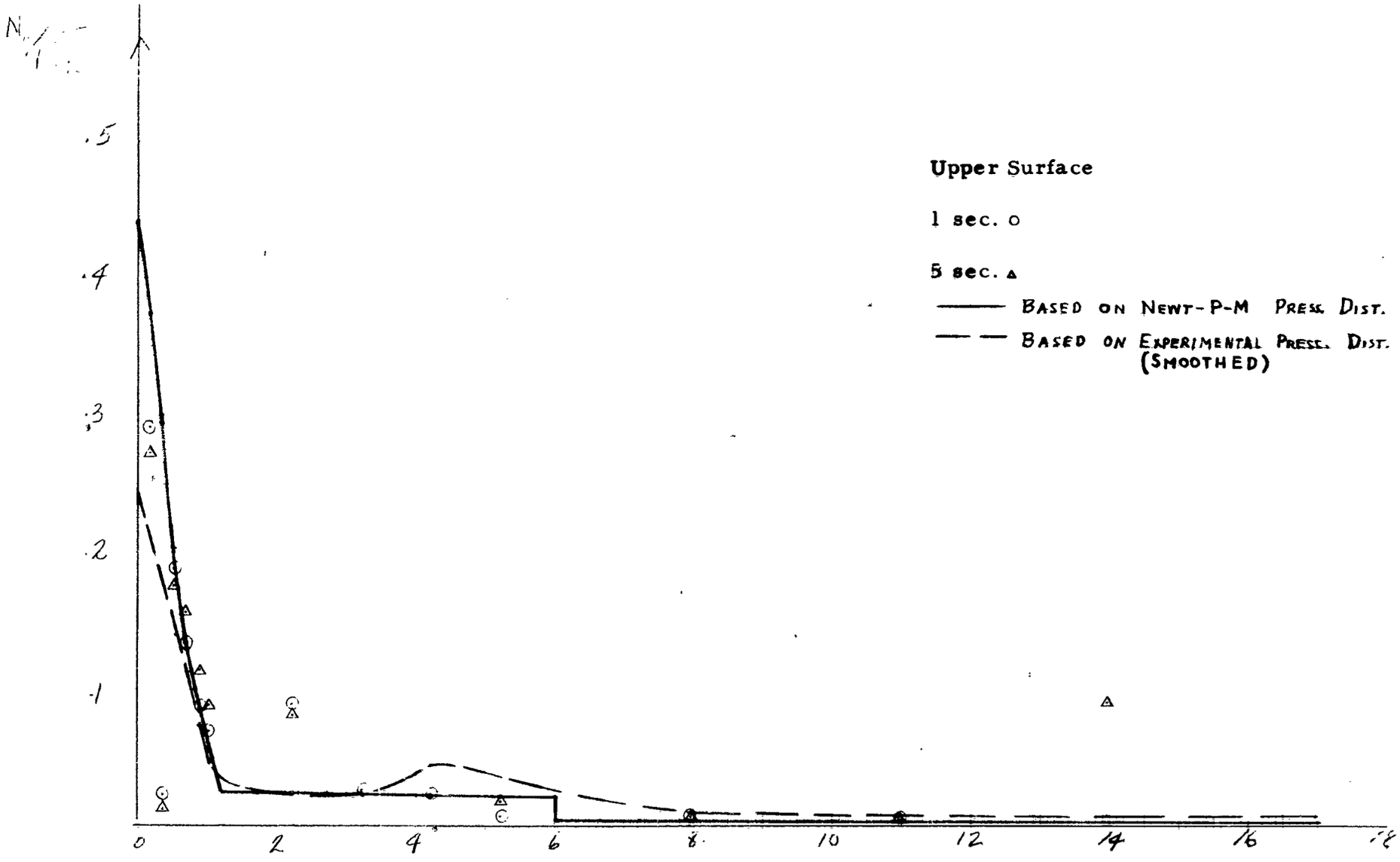

Figure 10. Experimental Heat Transfer Distribution on Two-Dimensional, Asymmetric, Blunt Body at Mach 8.08, $\alpha = 30^{\circ}$.

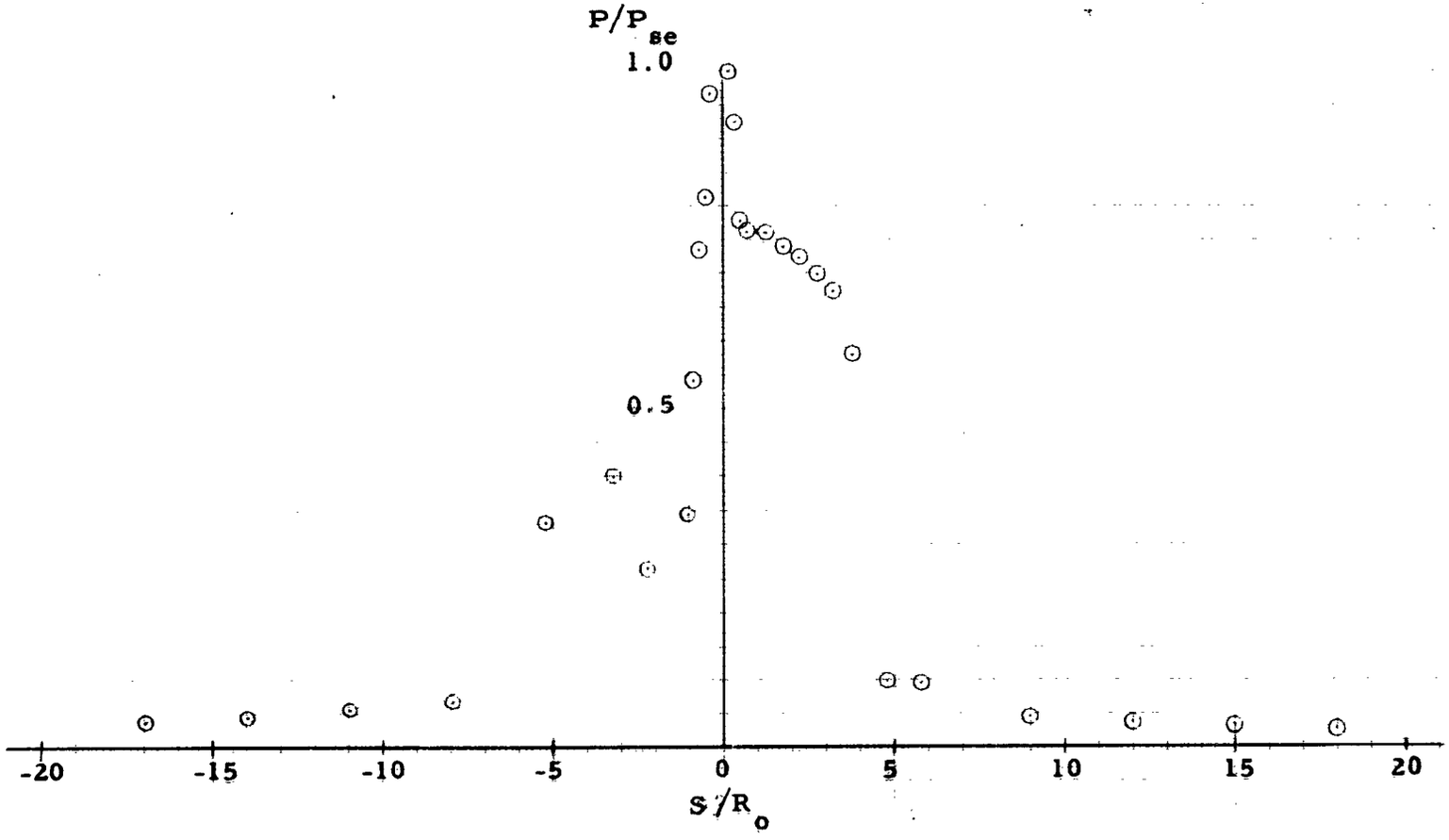

Figure 11. Experimental Pressure Distribution on Two-Dimensional, Asymmetric, Blunt Body at Mach 8.08, $\alpha = -3^{\circ}$.

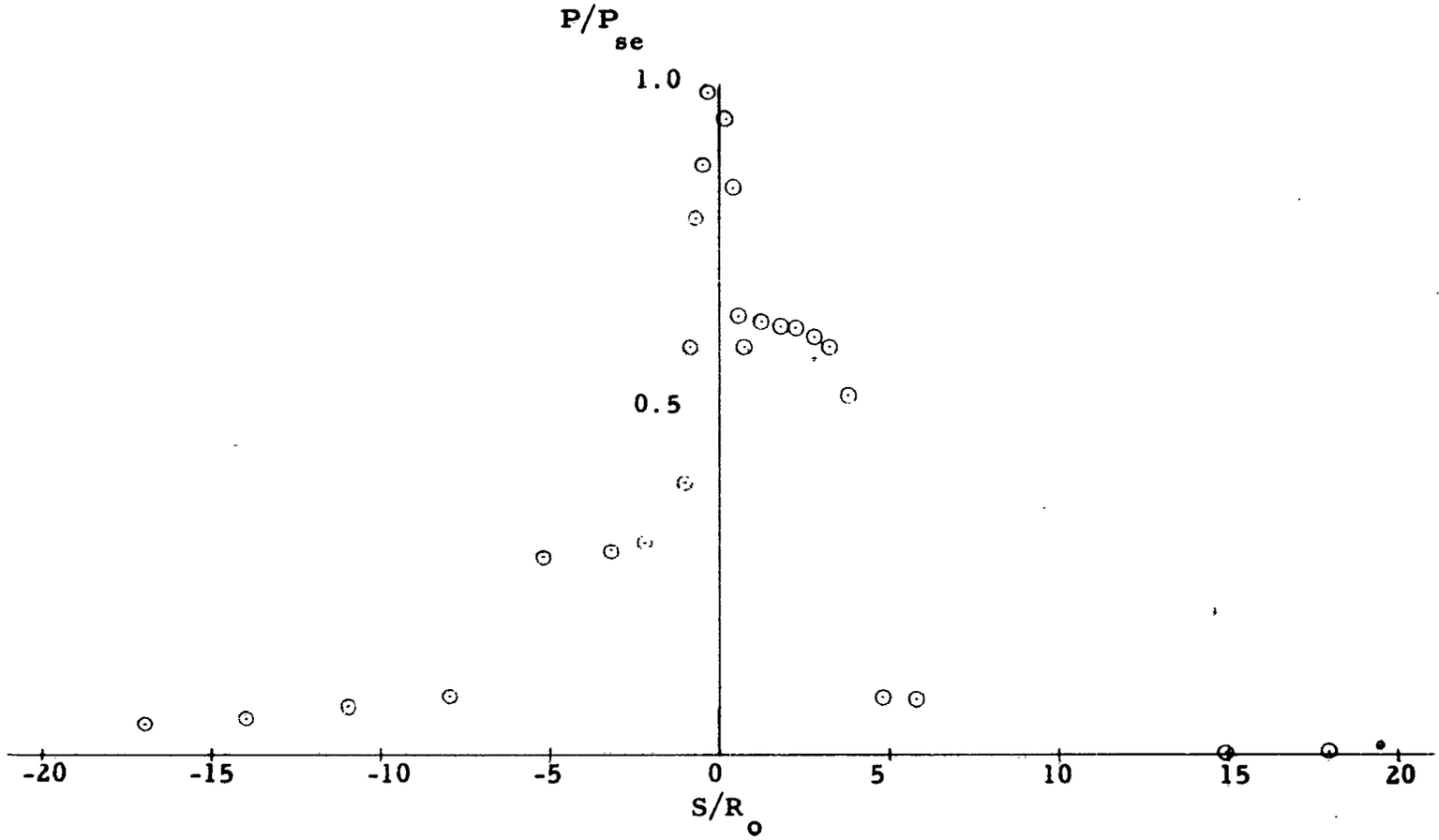

Figure 12. Experimental Pressure Distribution on Two-Dimensional, Asymmetric, Blunt Body at Mach 8.08, $\alpha = -6^{o}$

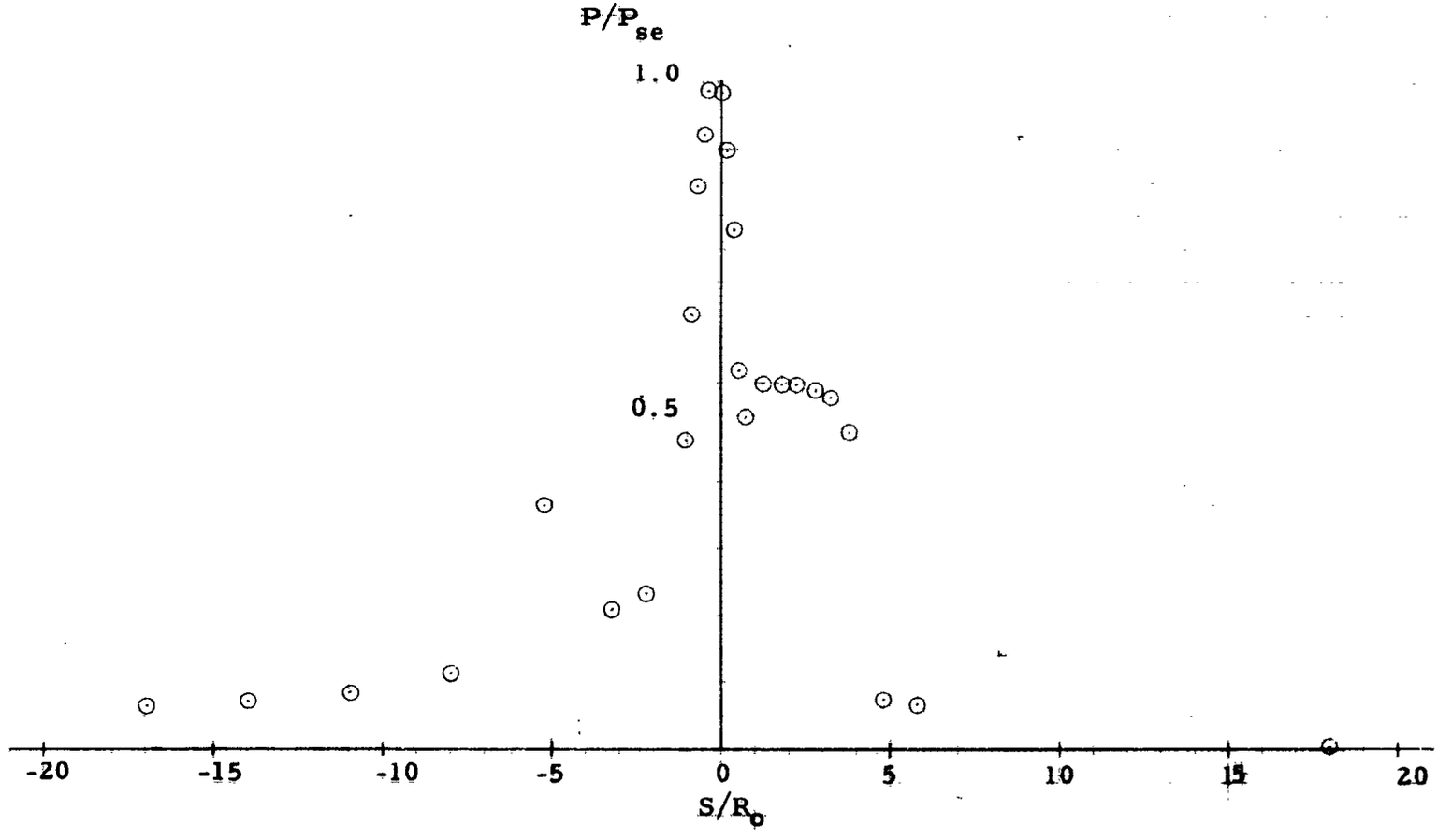

Figure 13. Experimental Pressure Distribution on Two-Dimensional, Asymmetric, Blunt Body at Mach 8.08, $\alpha = -9^{\circ}$.

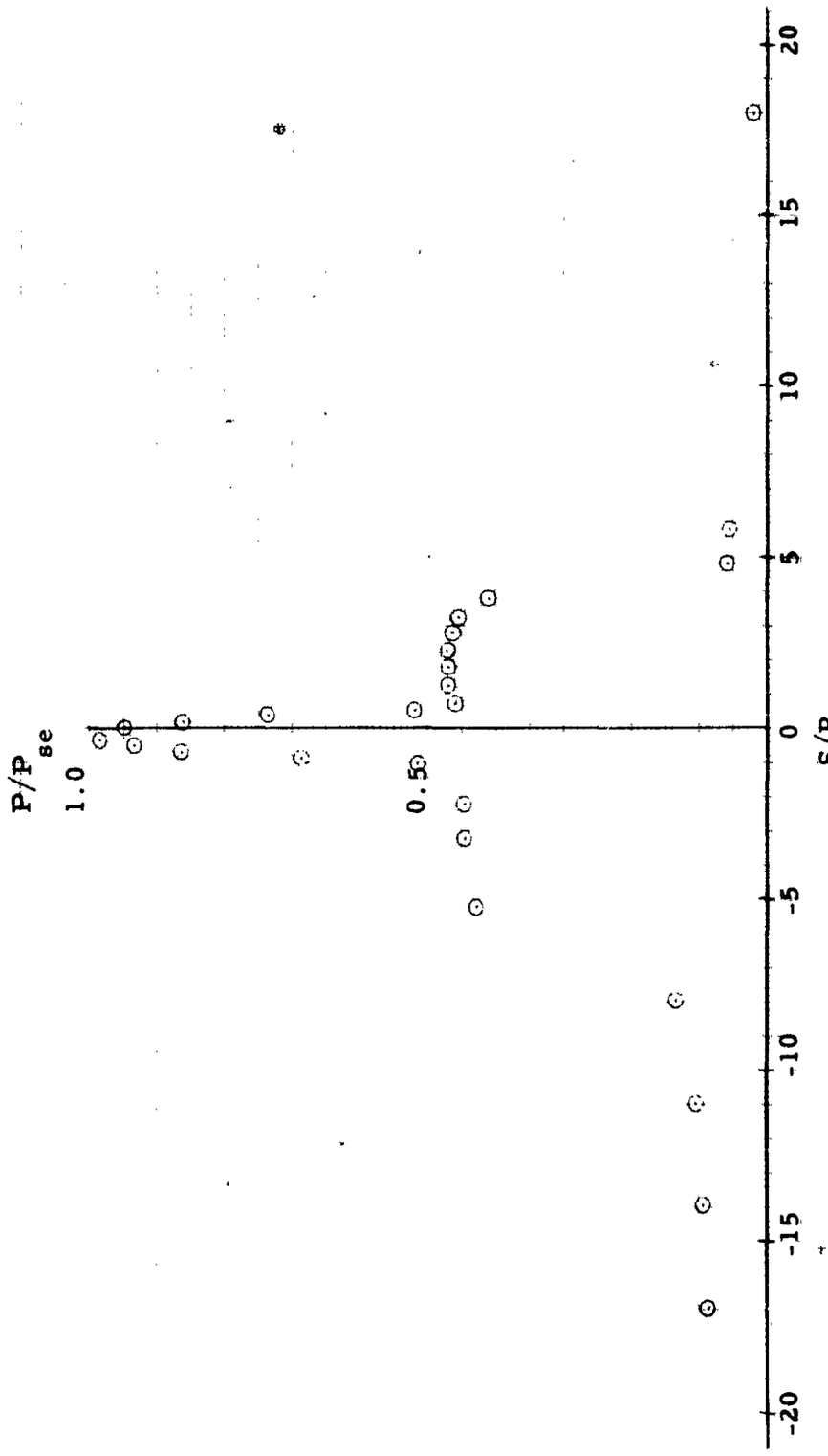

Figure 14. Experimental Pressure Distribution on Two-Dimensional, Asymmetric, Blunt Body at Mach 8.08, $\alpha = -12^{\circ}$.

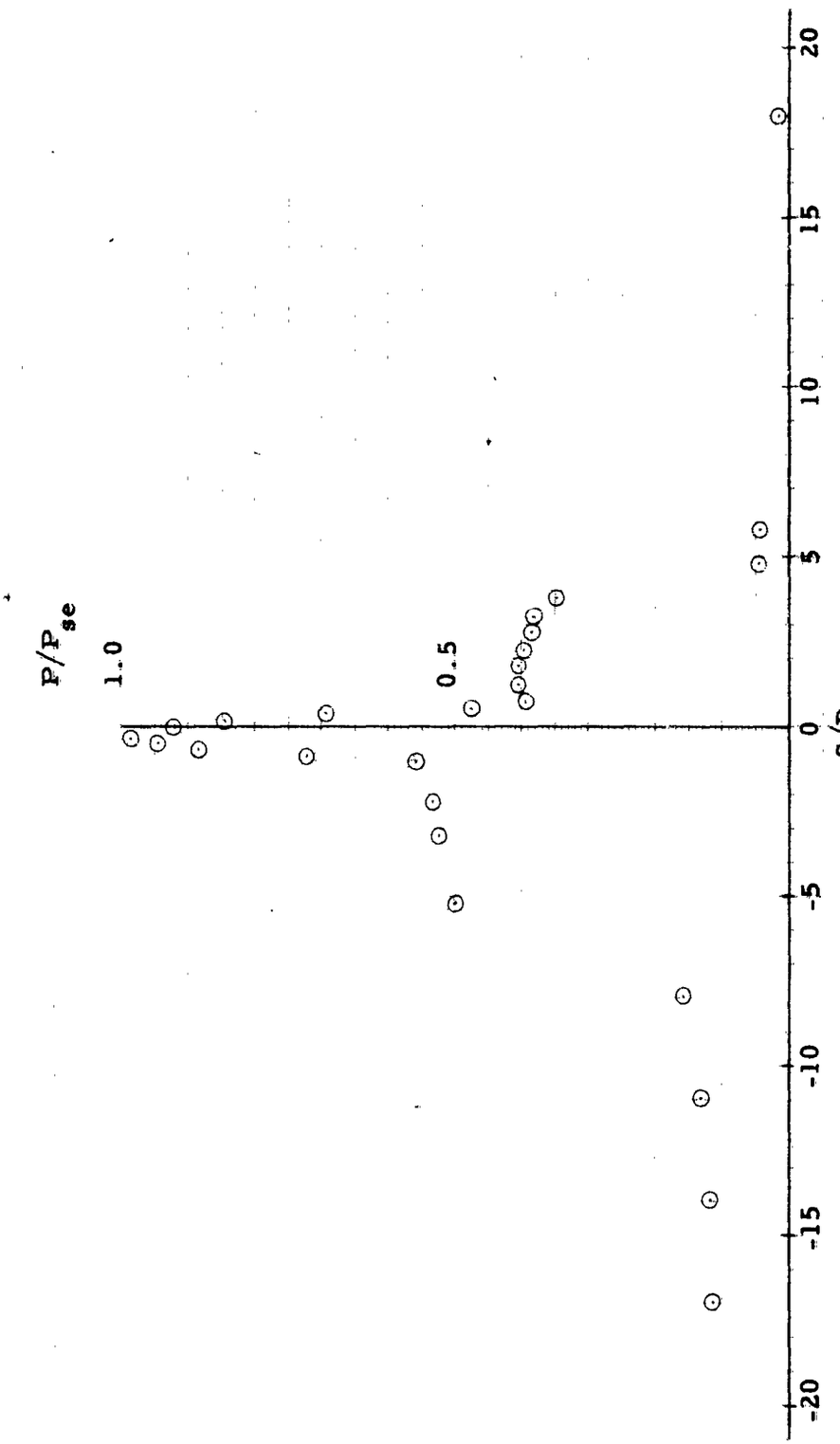

Figure 15. Experimental Pressure Distribution on Two-Dimensional, Asymmetric, Blunt Body at Mach 8.08, $\alpha = -15^{0}$

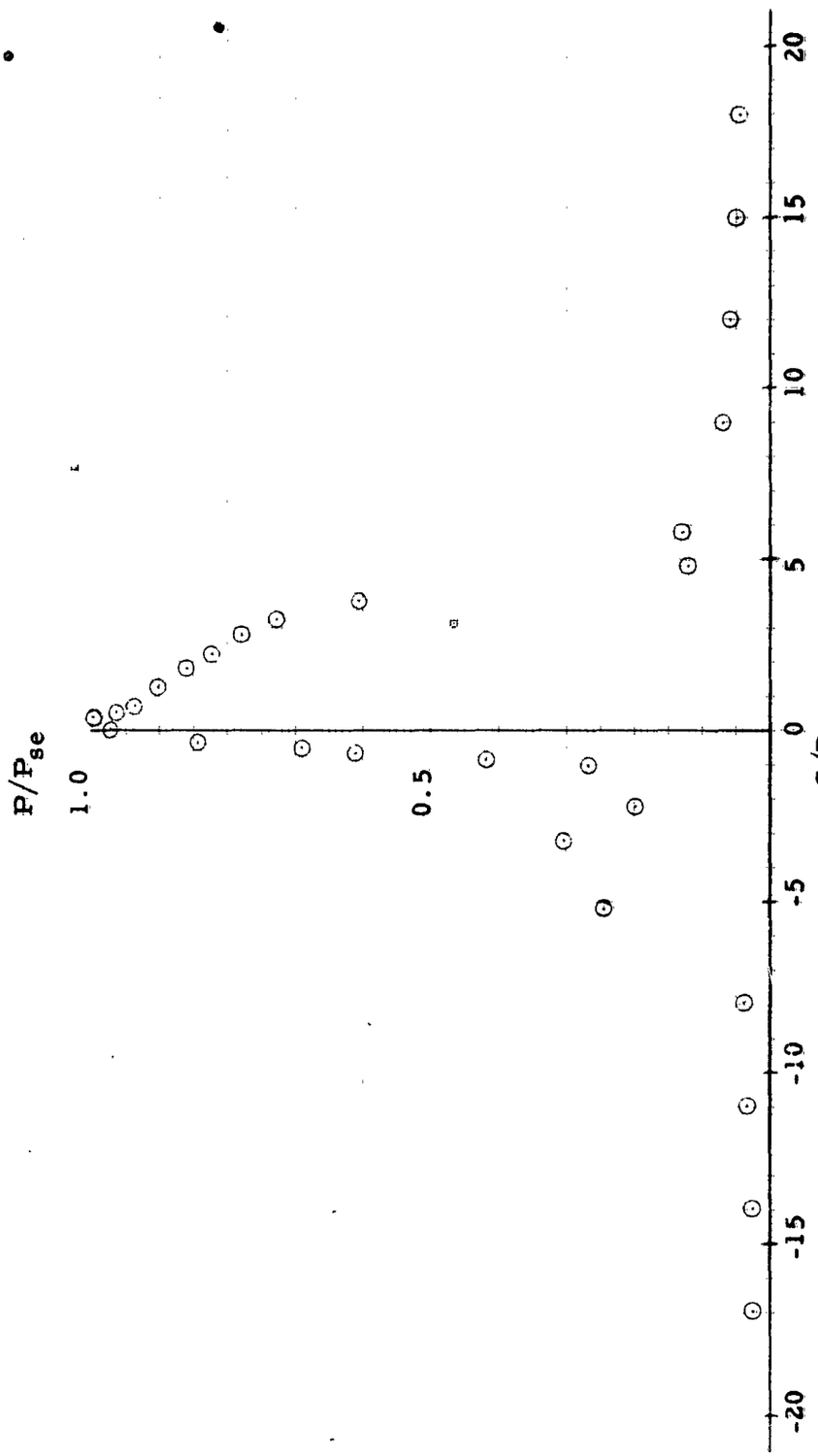

Figure 16. Experimental Pressure Distribution on Two-Dimensional, Asymmetric, Blunt Body at Mach 8.08, $\alpha = 3^{\circ}$.

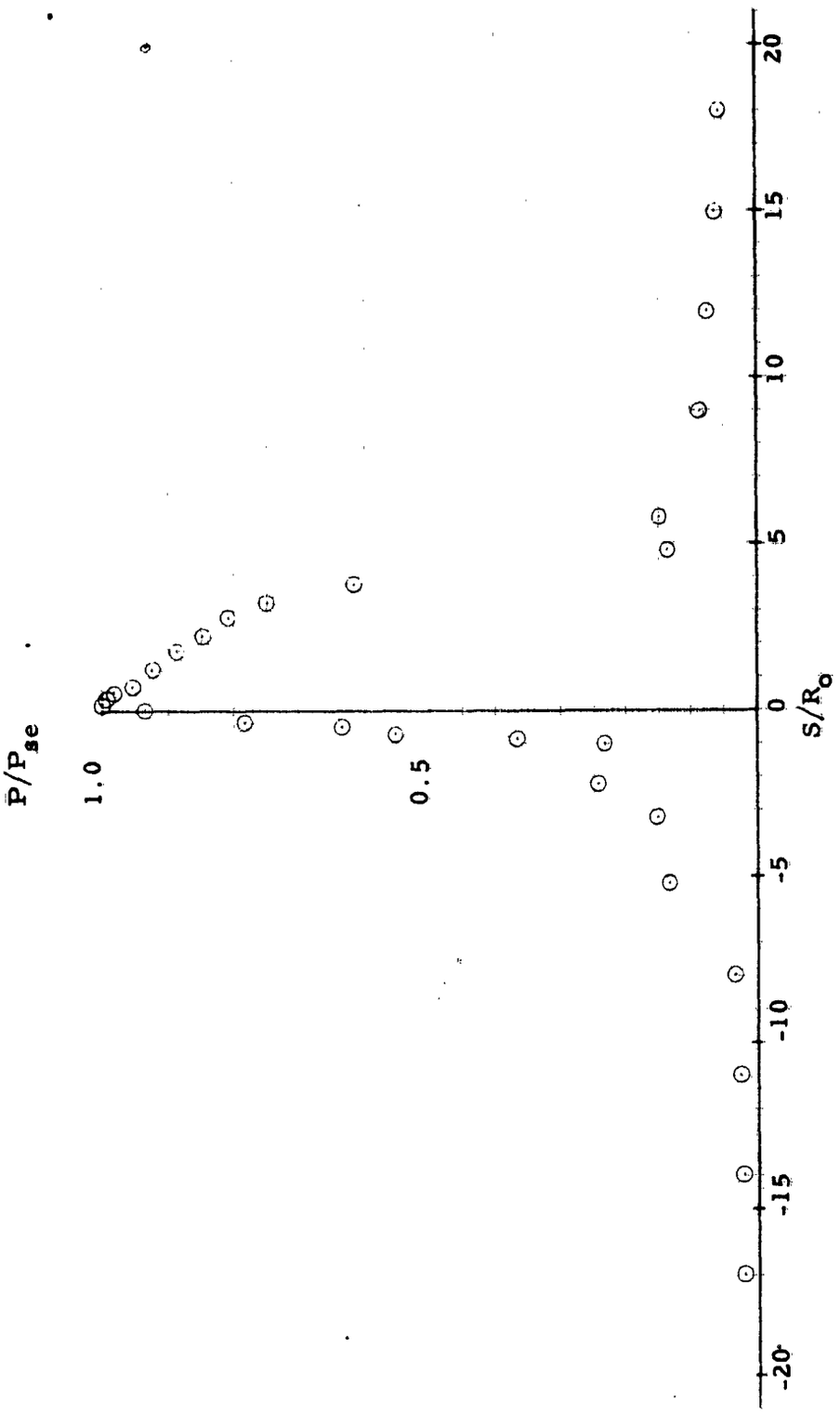

Figure 17. Experimental Pressure Distribution on Two-Dimensional, Asymmetric, Blunt Body at Mach 8.08, $\alpha = 6°$.

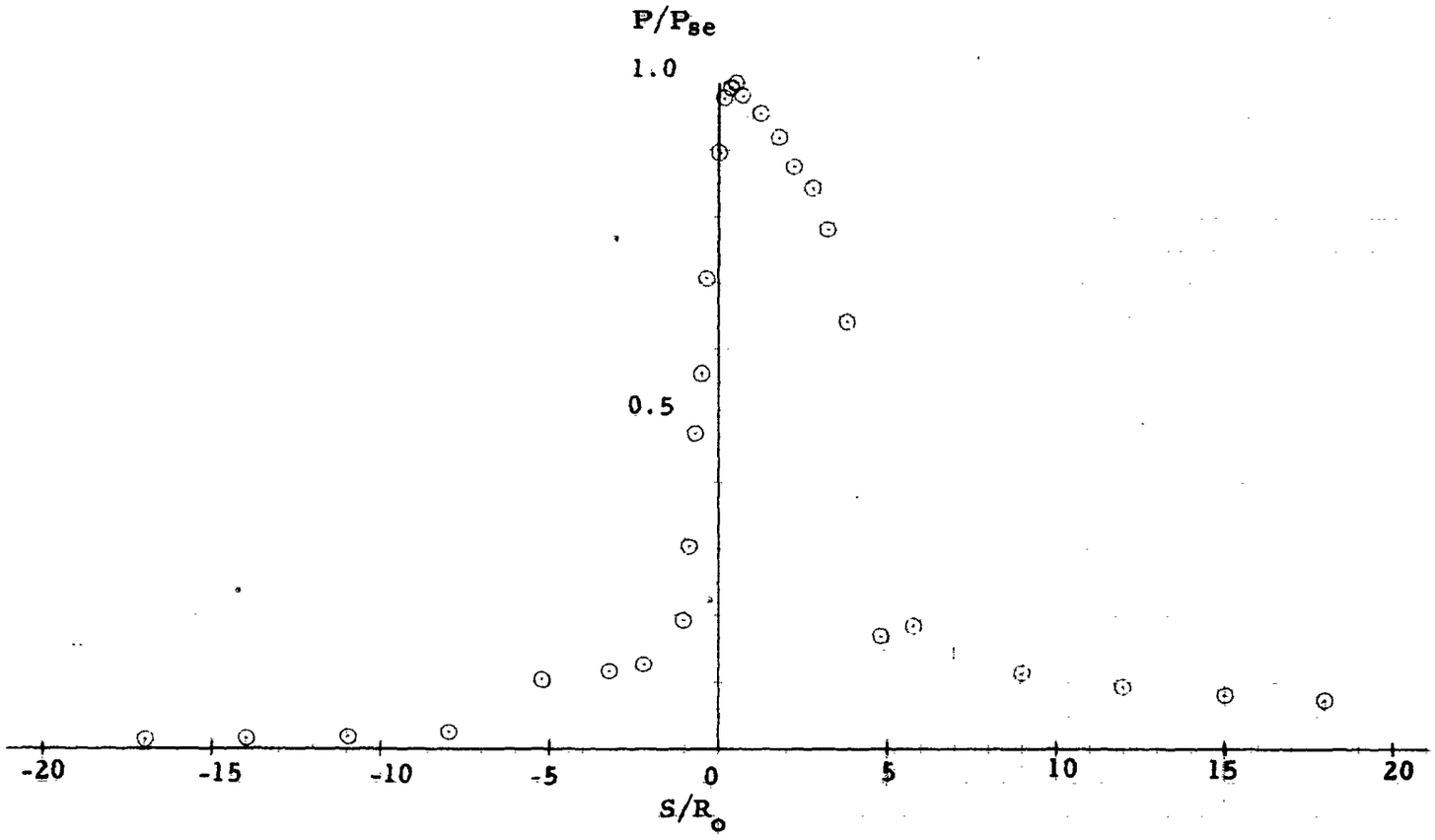

Figure 18. Experimental Pressure Distribution on Two-Dimensional, Asymmetric, Blunt Body at Mach 8.08, $\alpha = 10^{\circ}$.

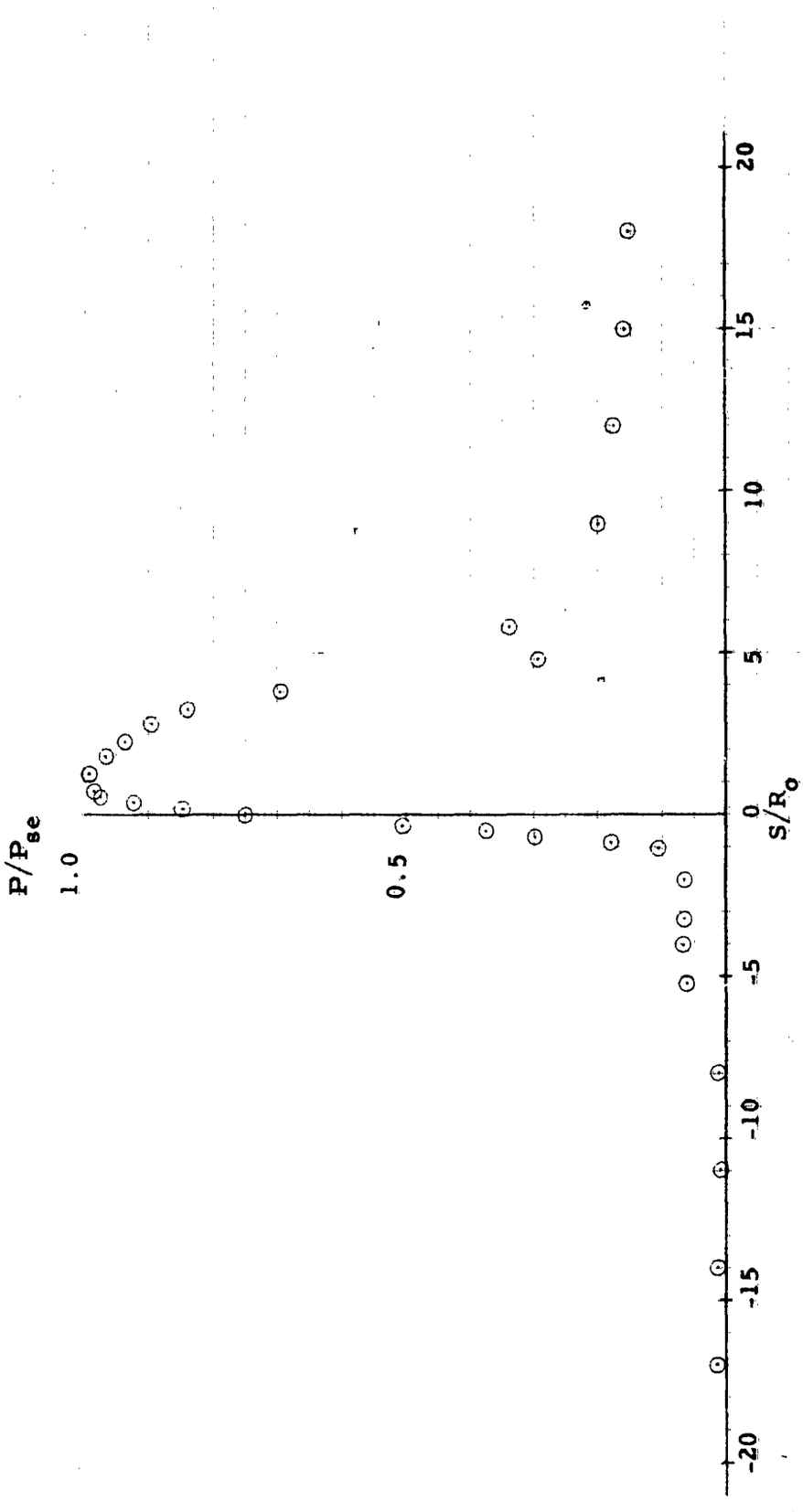

Figure 19. Experimental Pressure Distribution on Two-Dimensional, Asymmetric, Blunt Body at Mach 8.08, $\alpha = 20^{o}$.

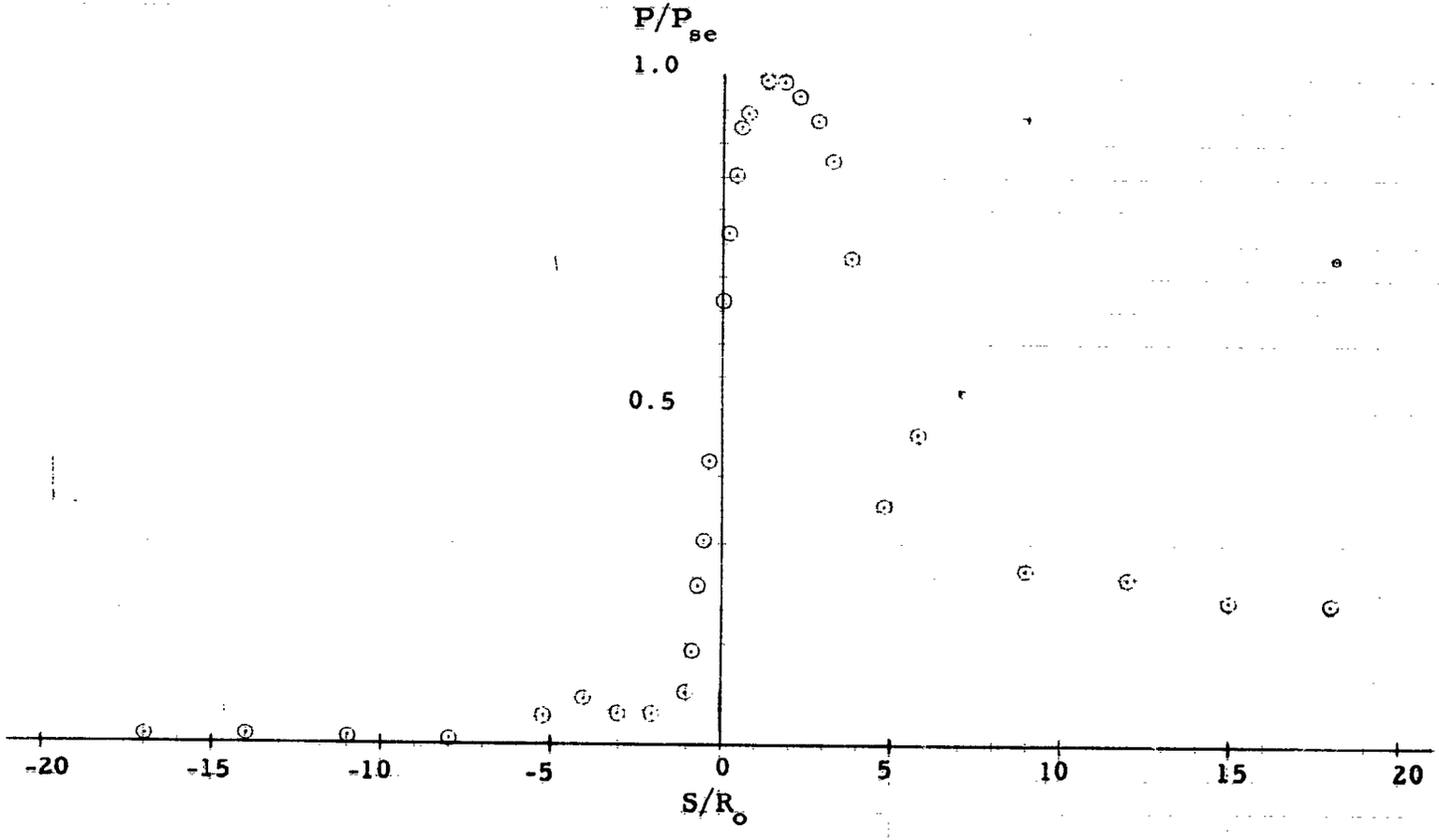

Figure 20. Experimental Pressure Distribution on Two-Dimensional, Asymmetric, Blunt Body at Mach 8.08, $\alpha = 25^{\circ}$.

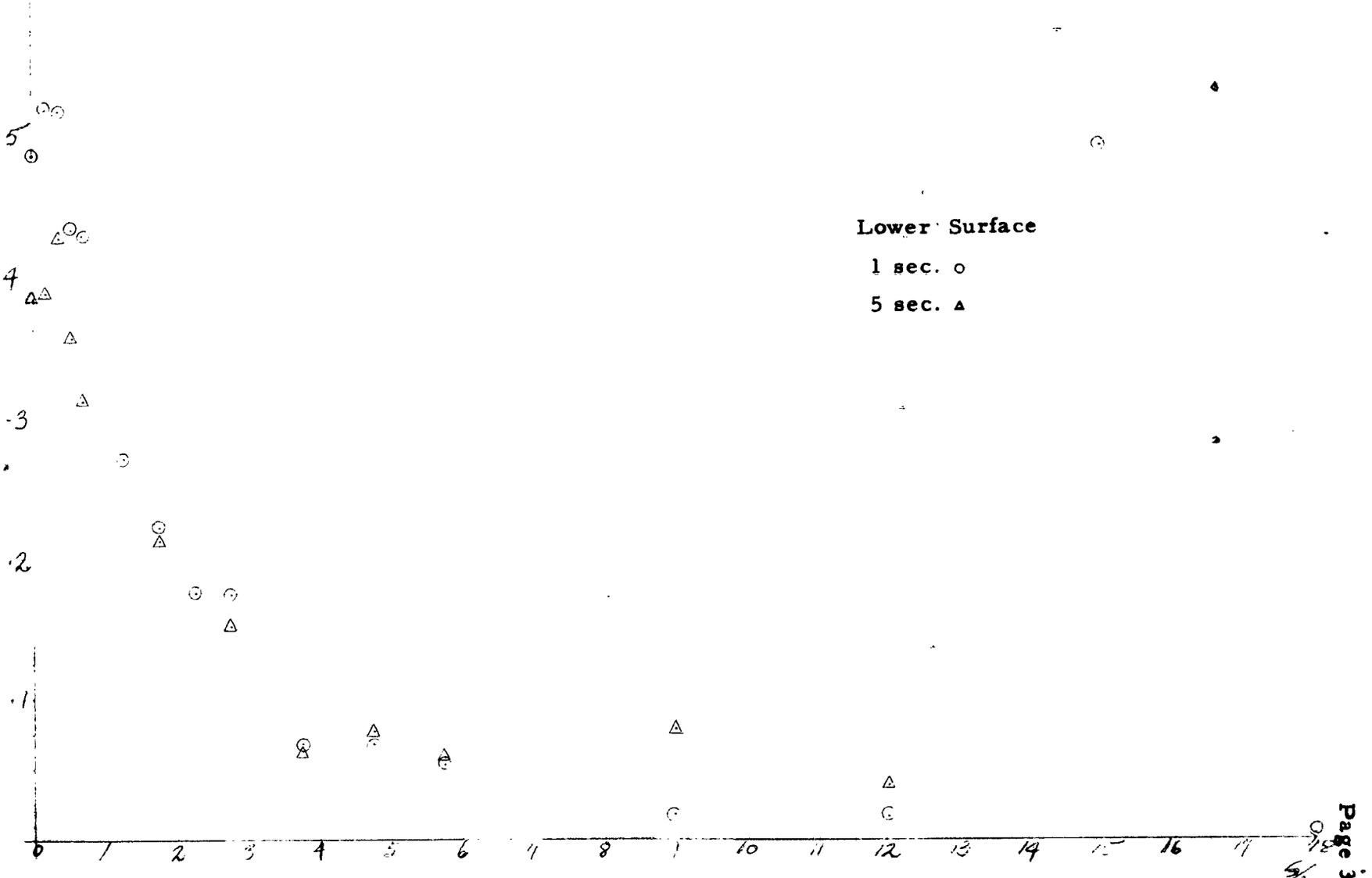

Figure 21. Experimental Heat Transfer Distribution on Two-Dimensional, Asymmetric, Blunt Body at Mach 8.08, $\alpha = -3$.

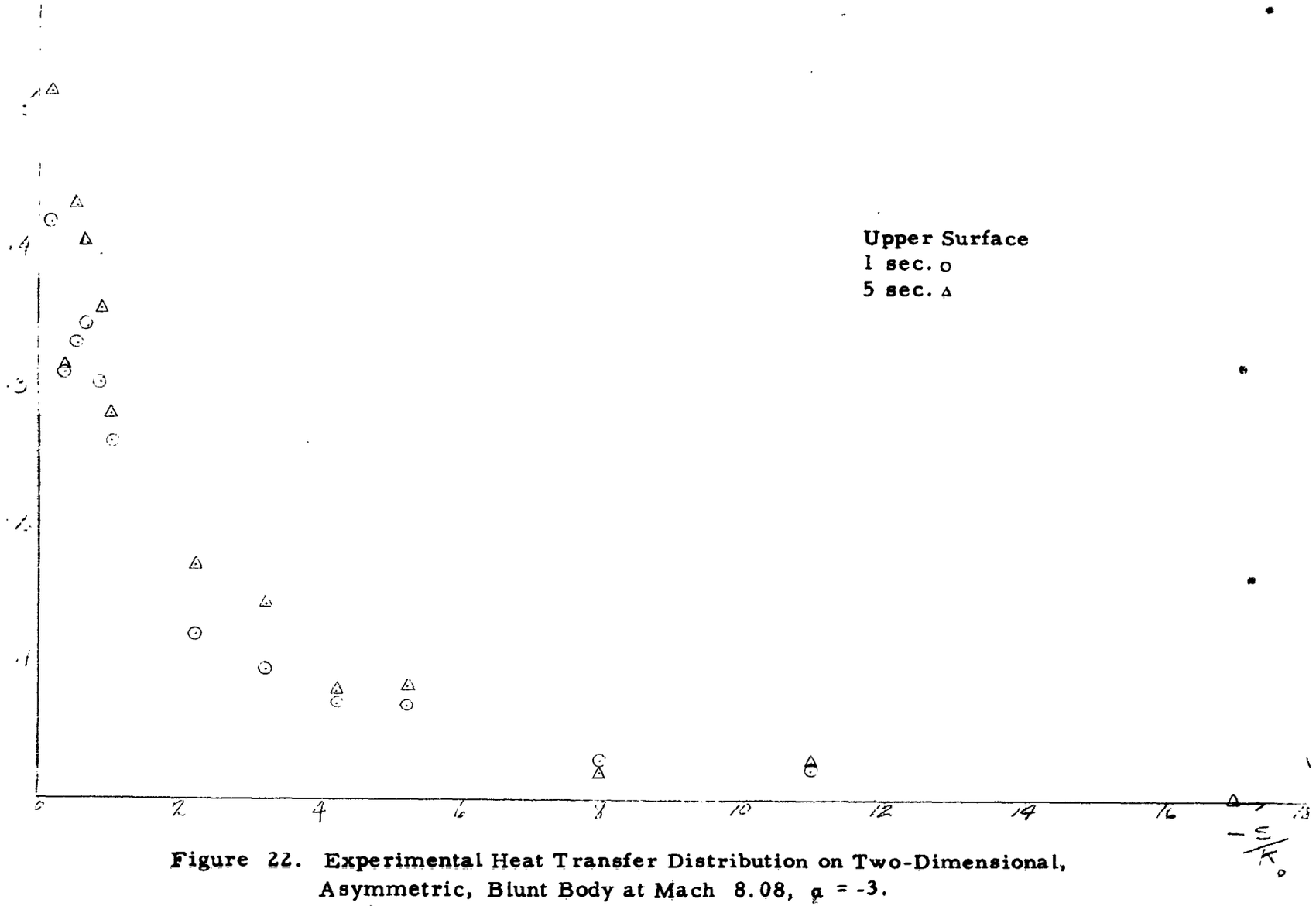

Figure 22. Experimental Heat Transfer Distribution on Two-Dimensional, Asymmetric, Blunt Body at Mach 8.08, α = -3.

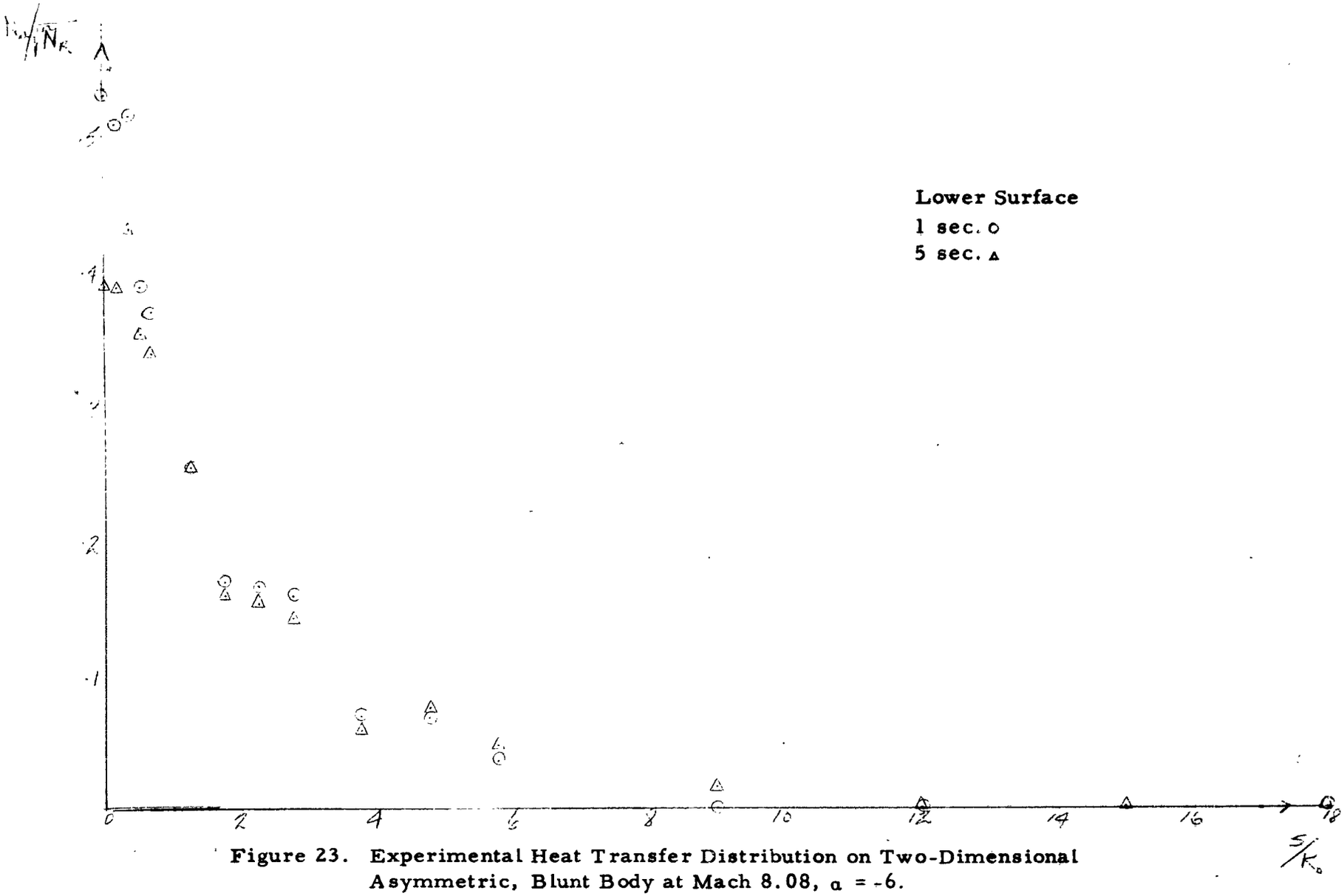

Figure 23. Experimental Heat Transfer Distribution on Two-Dimensional Asymmetric, Blunt Body at Mach 8.08, $\alpha = -6$.

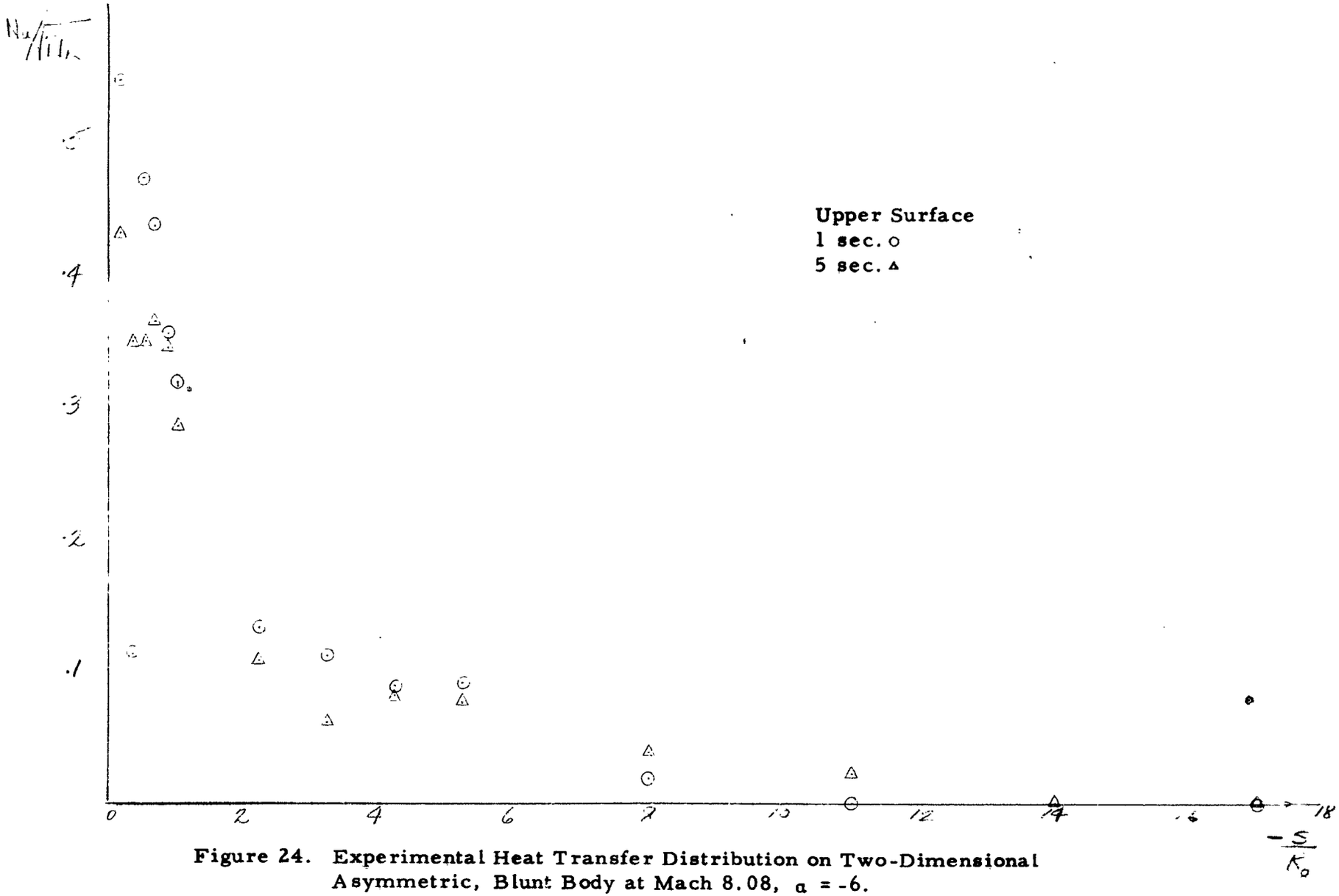

Figure 24. Experimental Heat Transfer Distribution on Two-Dimensional Asymmetric, Blunt Body at Mach 8.08, $\alpha = -6$.

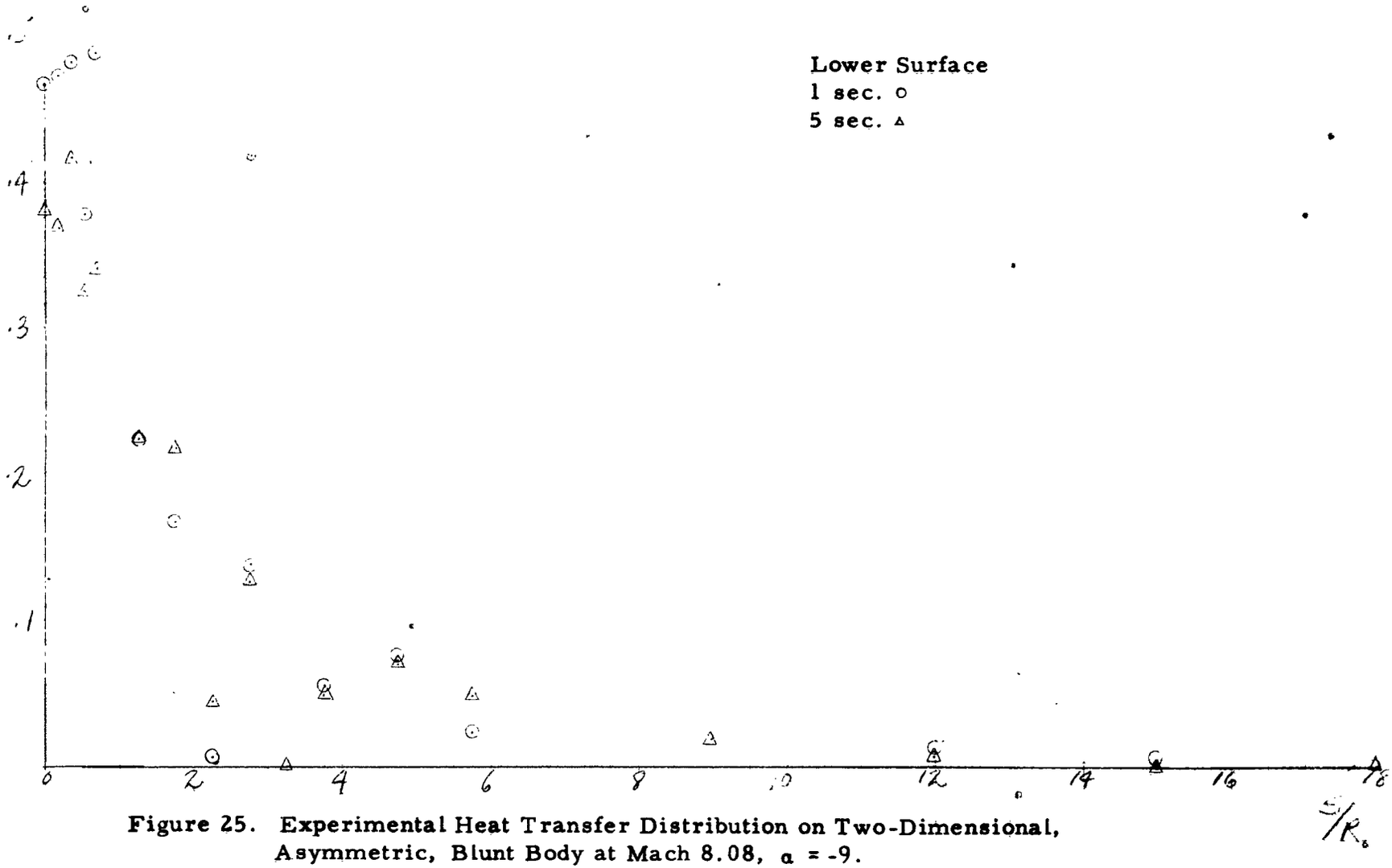

Figure 25. Experimental Heat Transfer Distribution on Two-Dimensional, Asymmetric, Blunt Body at Mach 8.08, $\alpha = -9$.

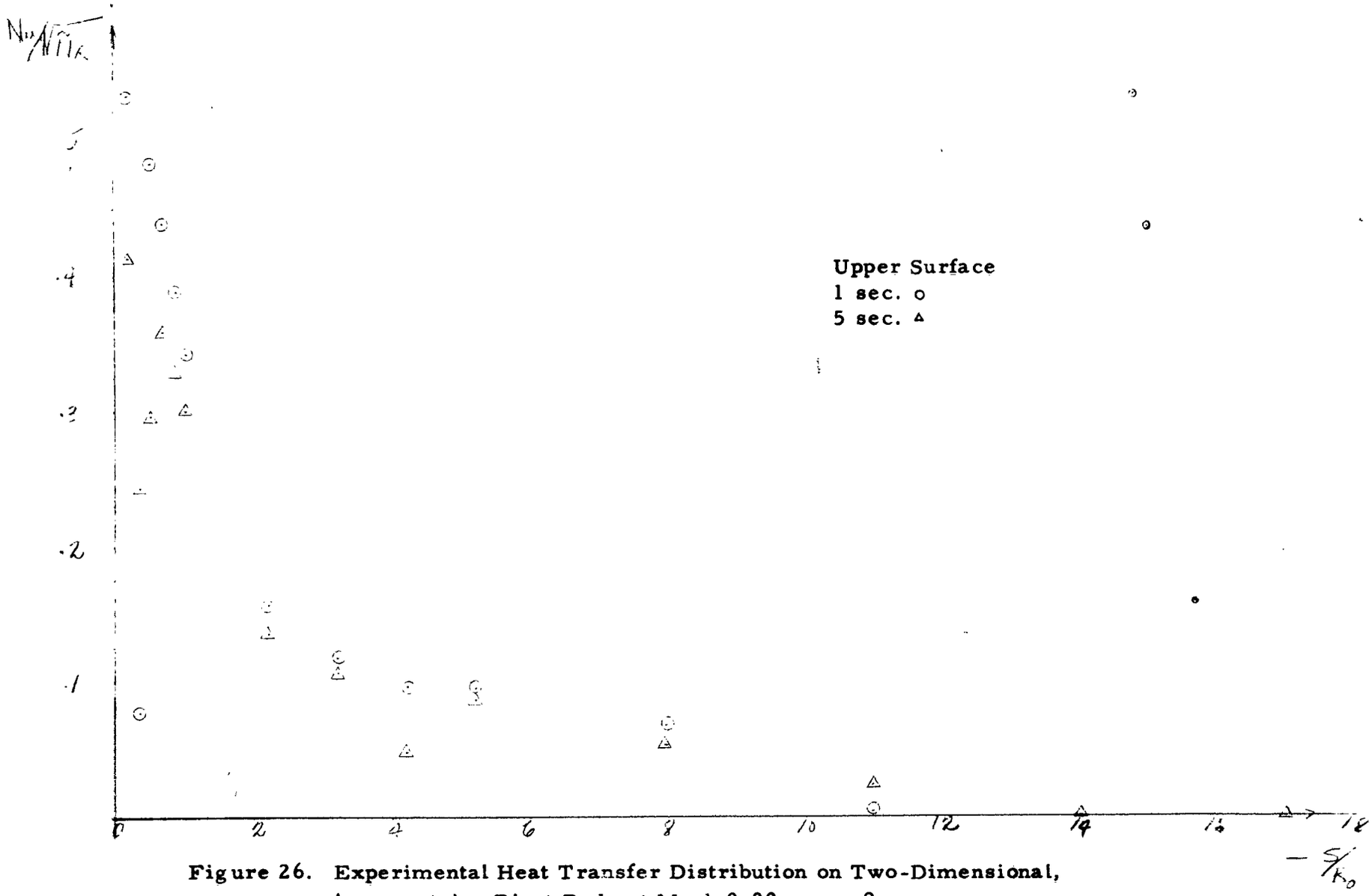

Figure 26. Experimental Heat Transfer Distribution on Two-Dimensional, Asymmetric, Blunt Body at Mach 8.08, α = -9.

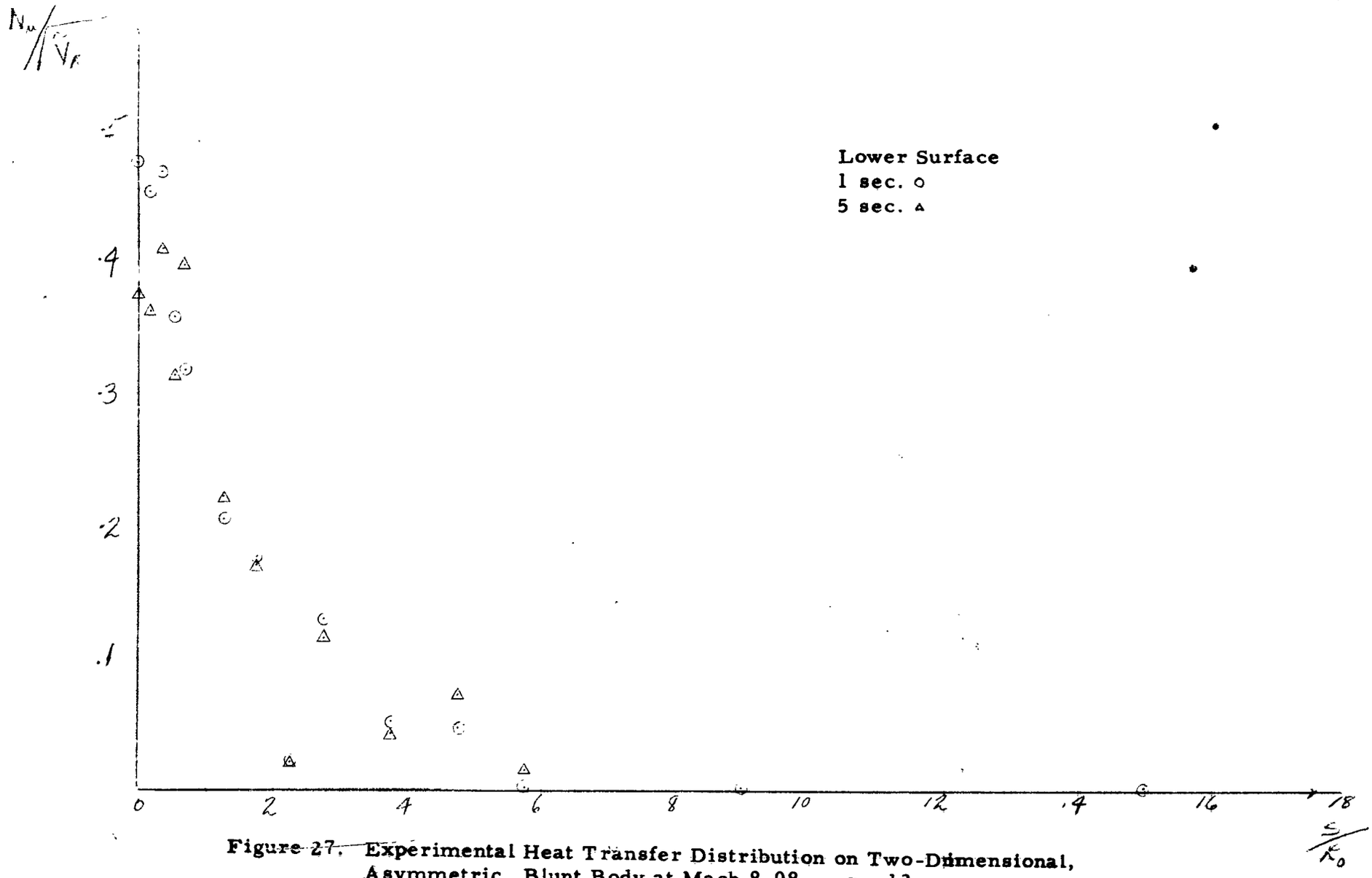

Figure 27. Experimental Heat Transfer Distribution on Two-Dimensional, Asymmetric, Blunt Body at Mach 8.08, α = -12.

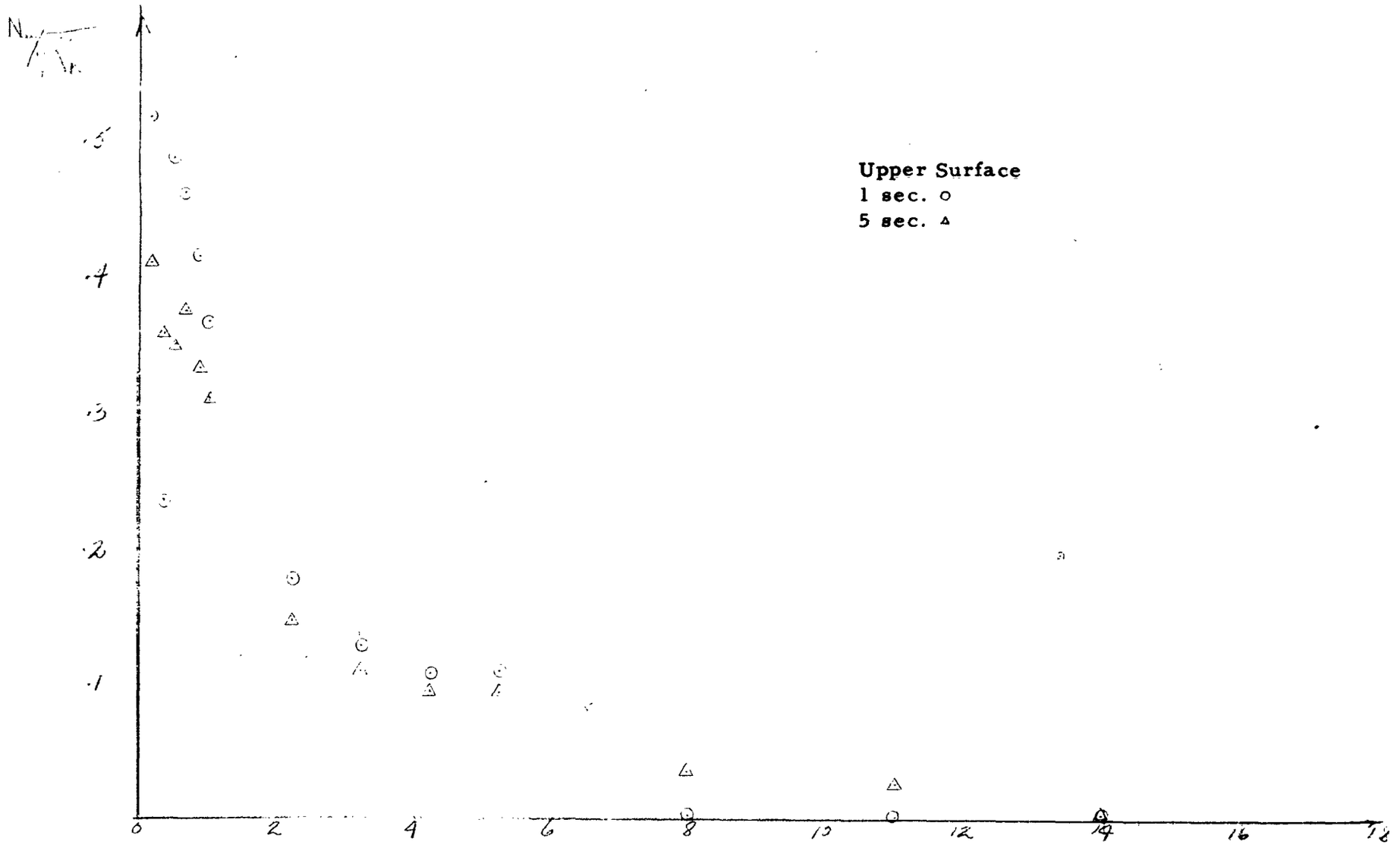

Figure 28. Experimental Heat Transfer Distribution on Two-Dimensional, Asymmetric, Blunt Body at Mach 8.08, $\alpha = -12$.

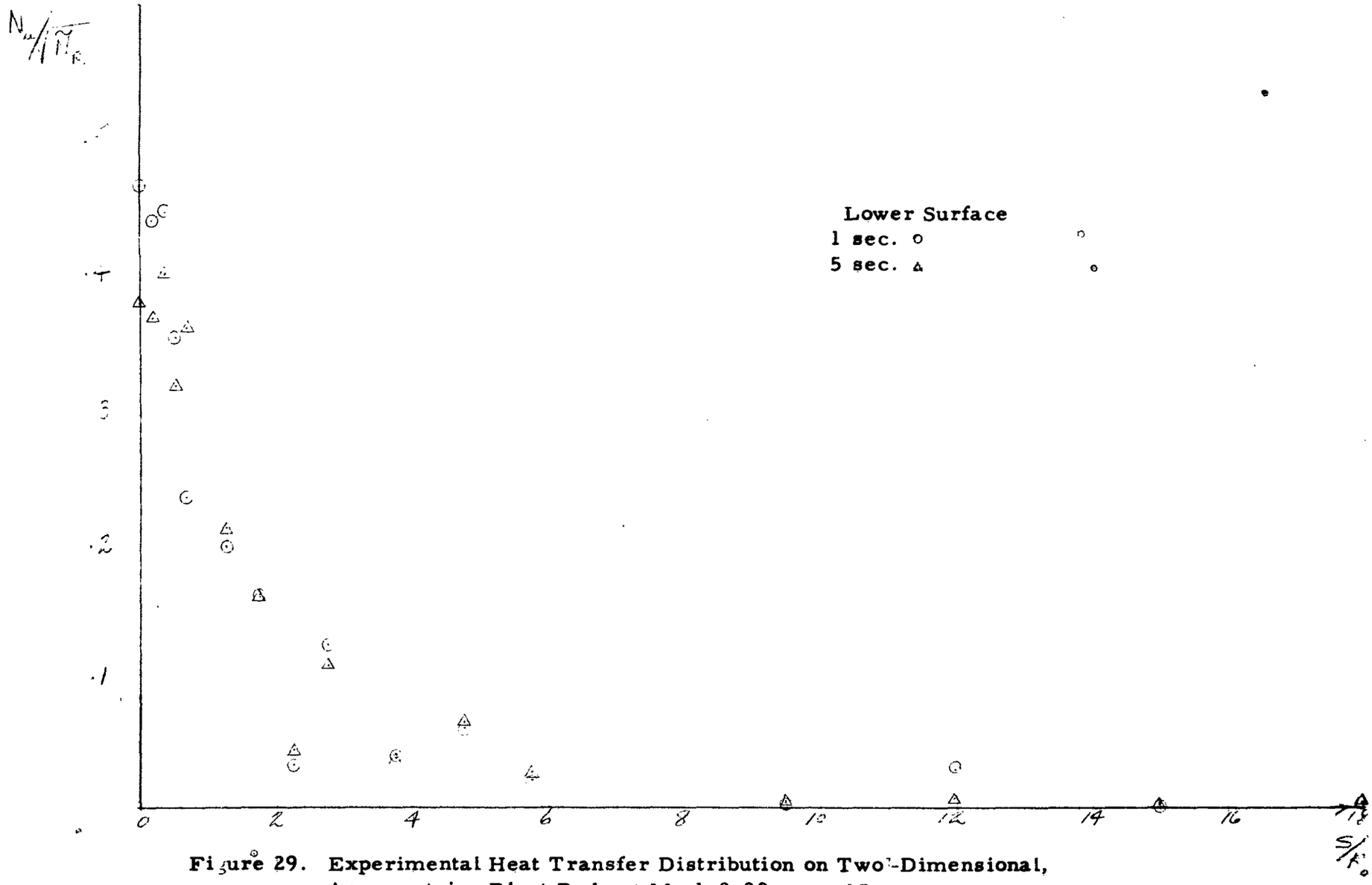

Figure 29. Experimental Heat Transfer Distribution on Two-Dimensional, Asymmetric, Blunt Body at Mach 8.08, $\alpha = -15$.

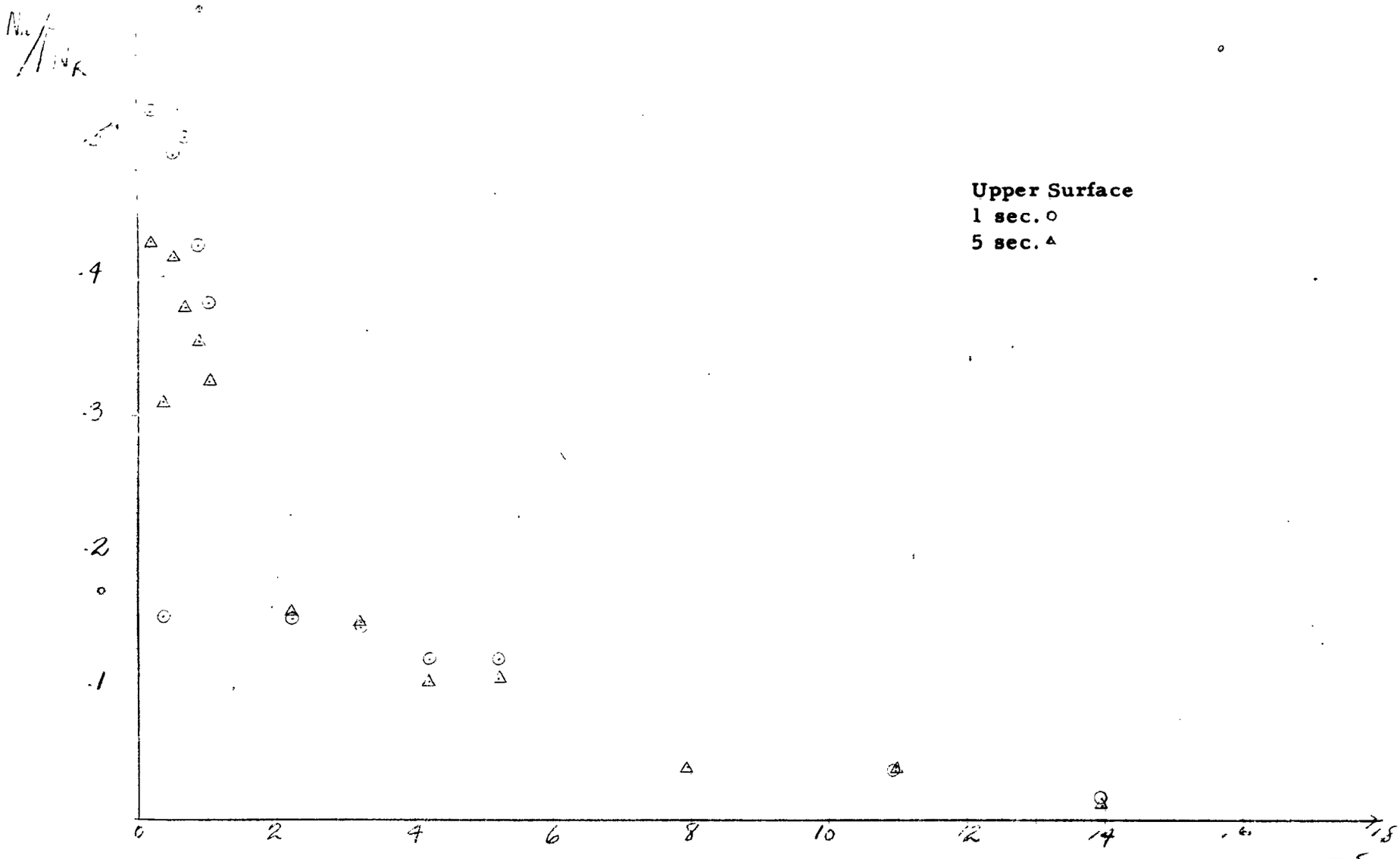

Figure 30. Experimental Heat Transfer Distribution on Two-Dimensional, Asymmetric, Blunt Body at Mach 8.08, $\alpha = -15$.

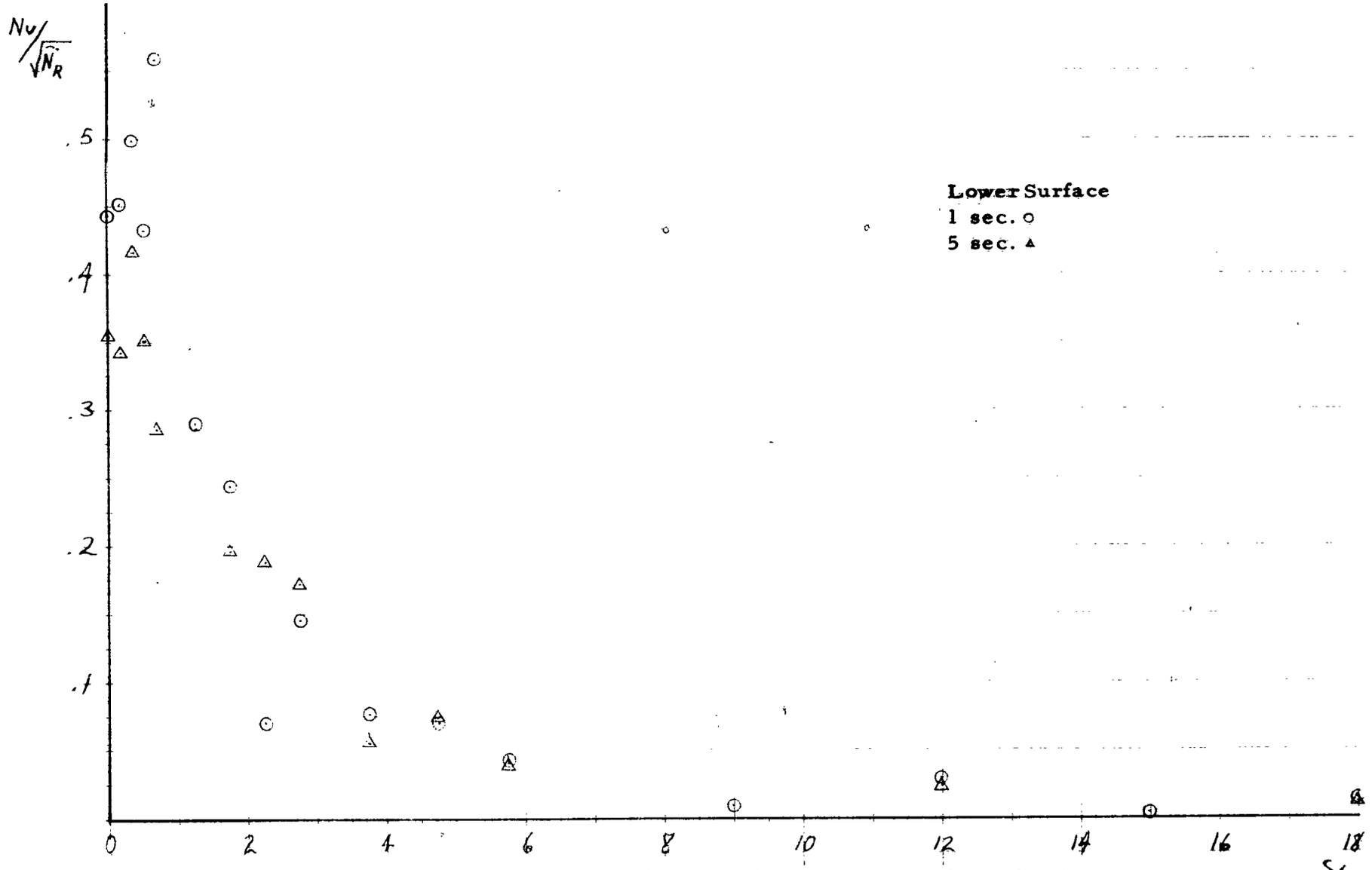

Figure 31. Experimental Heat Transfer Distribution on Two-Dimensional, Asymmetric, Blunt Body at Mach 8.08, $\alpha = 3^{\circ}$.

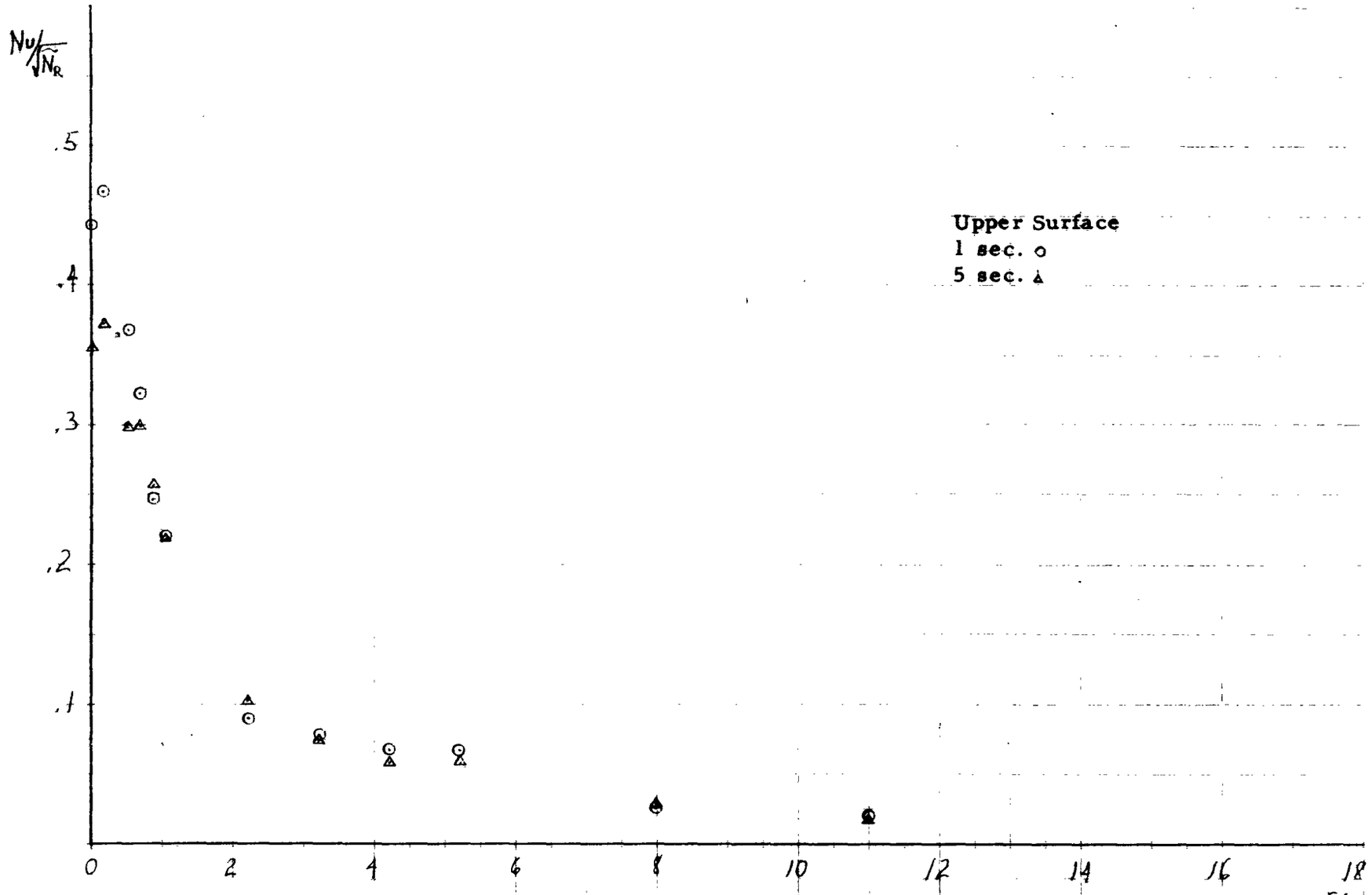

Figure 32. Experimental Heat Transfer Distribution on Two-Dimensional, Asymmetric, Blunt Body at Mach 8.08, $\alpha = 3^{\circ}$.

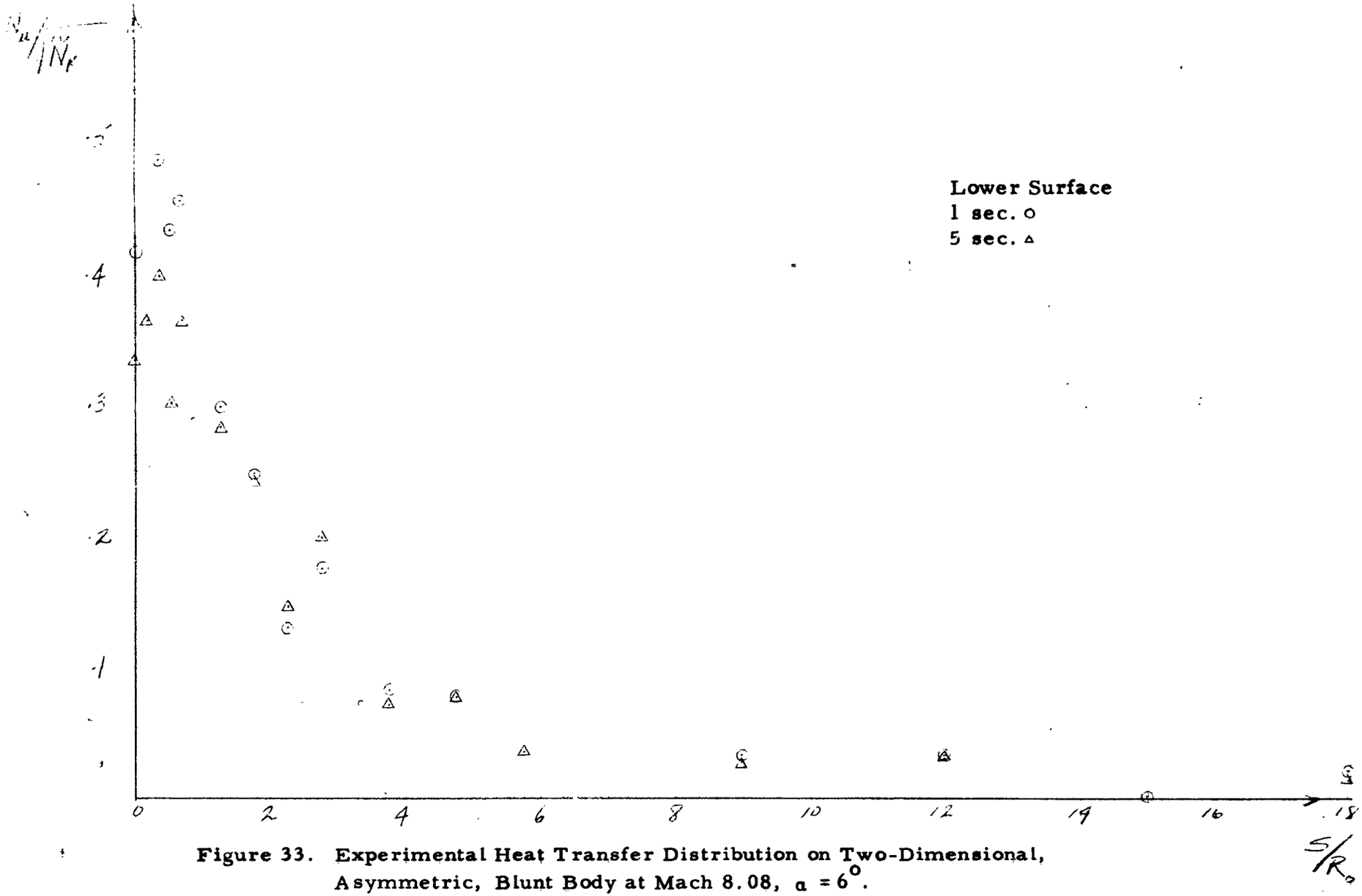

Figure 33. Experimental Heat Transfer Distribution on Two-Dimensional, Asymmetric, Blunt Body at Mach 8.08, $\alpha = 6^{o}$.

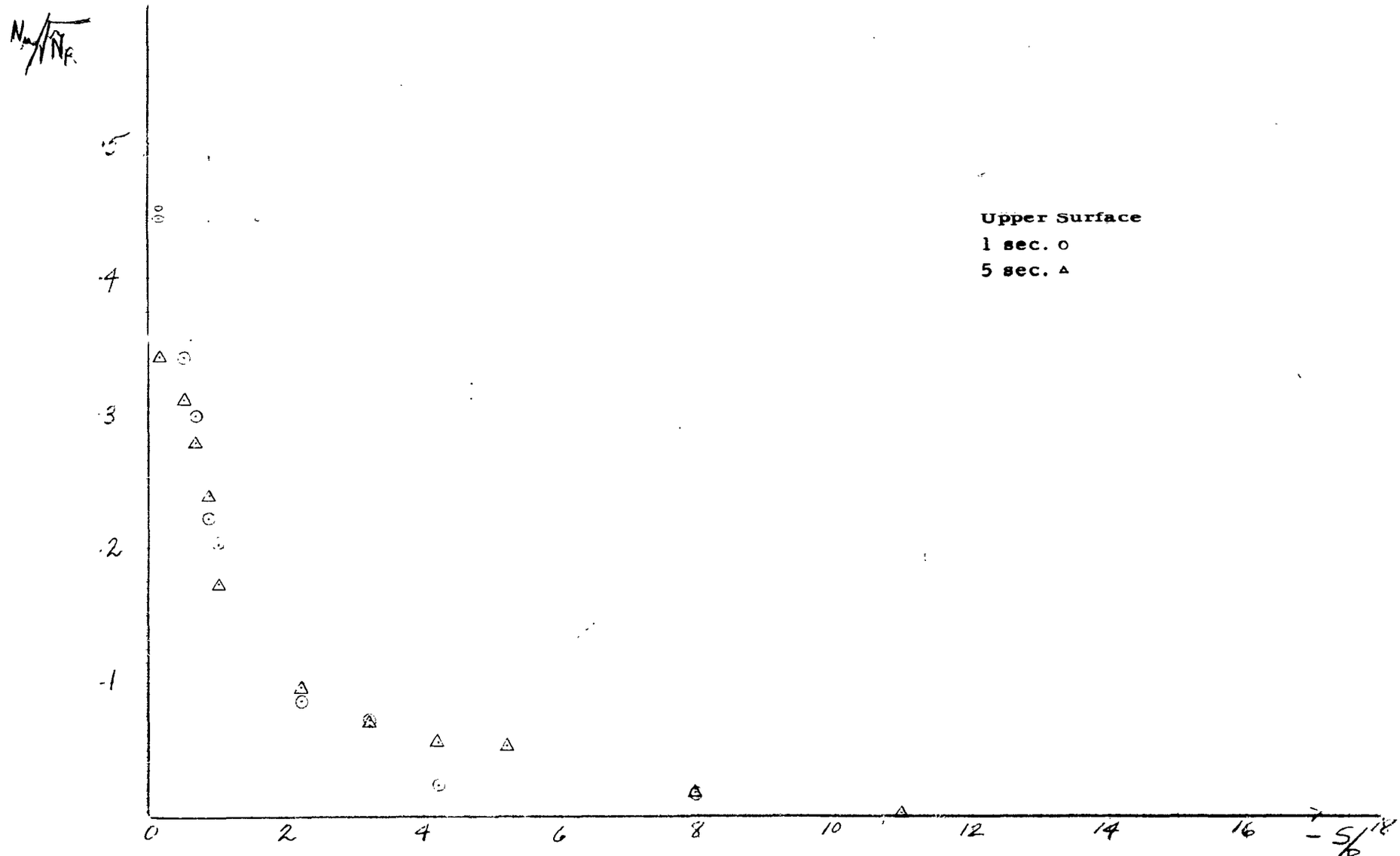

Figure 34. Experimental Heat Transfer Distribution on Two-Dimensional, Asymmetric, Blunt Body at Mach 8.08, $\alpha = 6$.

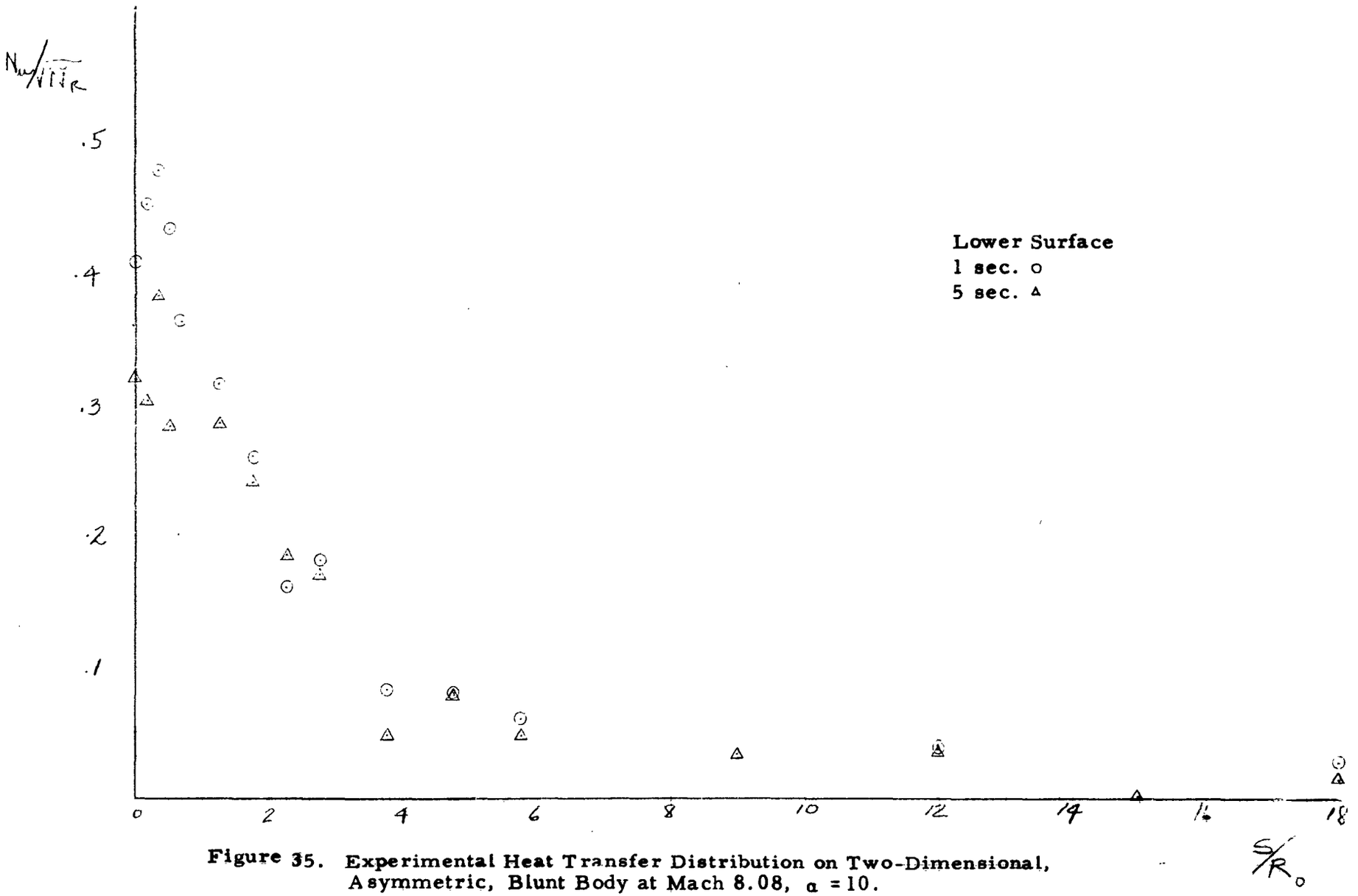

Figure 35. Experimental Heat Transfer Distribution on Two-Dimensional, Asymmetric, Blunt Body at Mach 8.08, $\alpha = 10$.

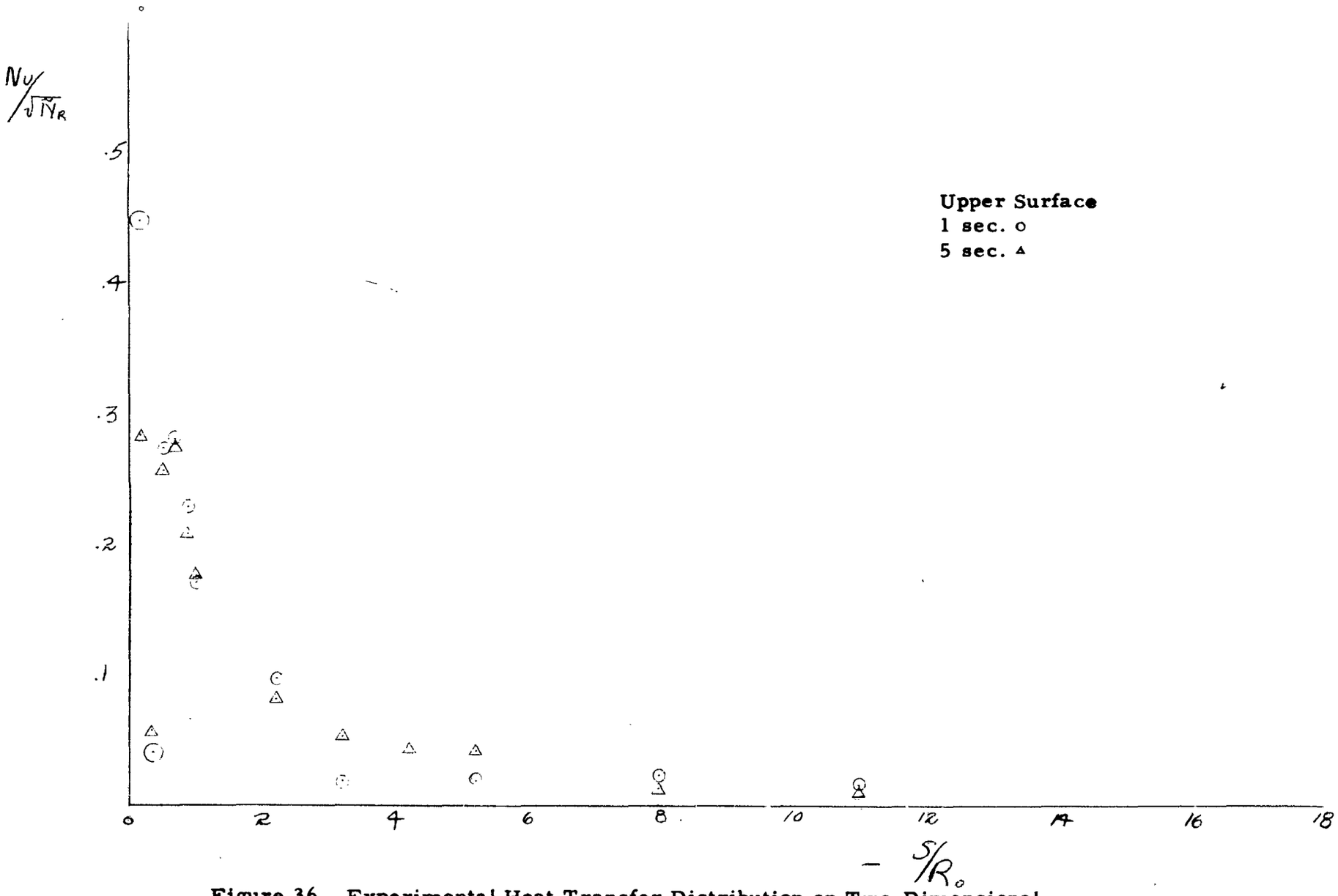

Figure 36. Experimental Heat Transfer Distribution on Two-Dimensional, Asymmetric, Blunt Body at Mach 8.08, $\alpha = 10$.

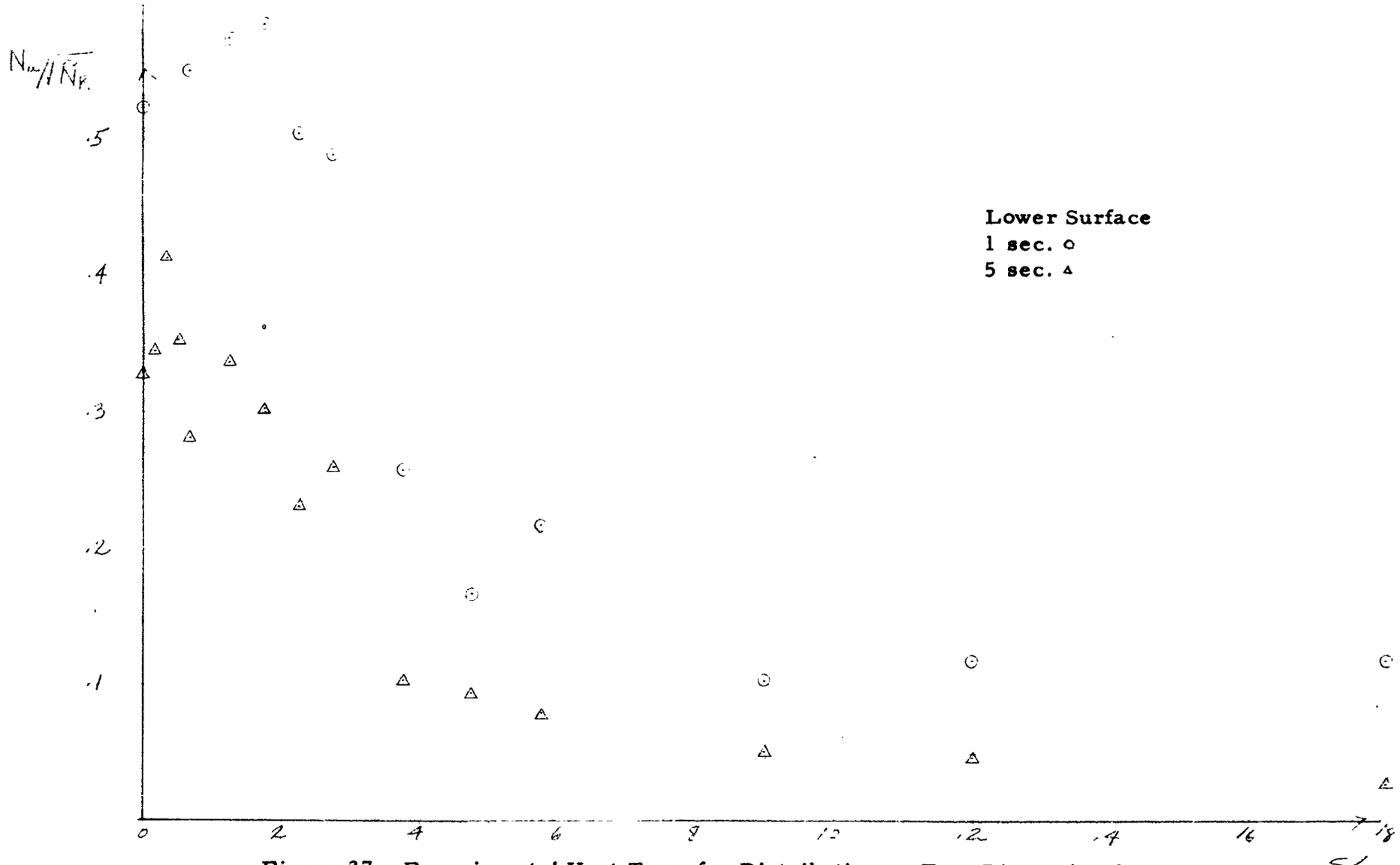

Figure 37. Experimental Heat Transfer Distribution on Two-Dimensional, Asymmetric, Blunt Body at Mach 8.08, α = 20.

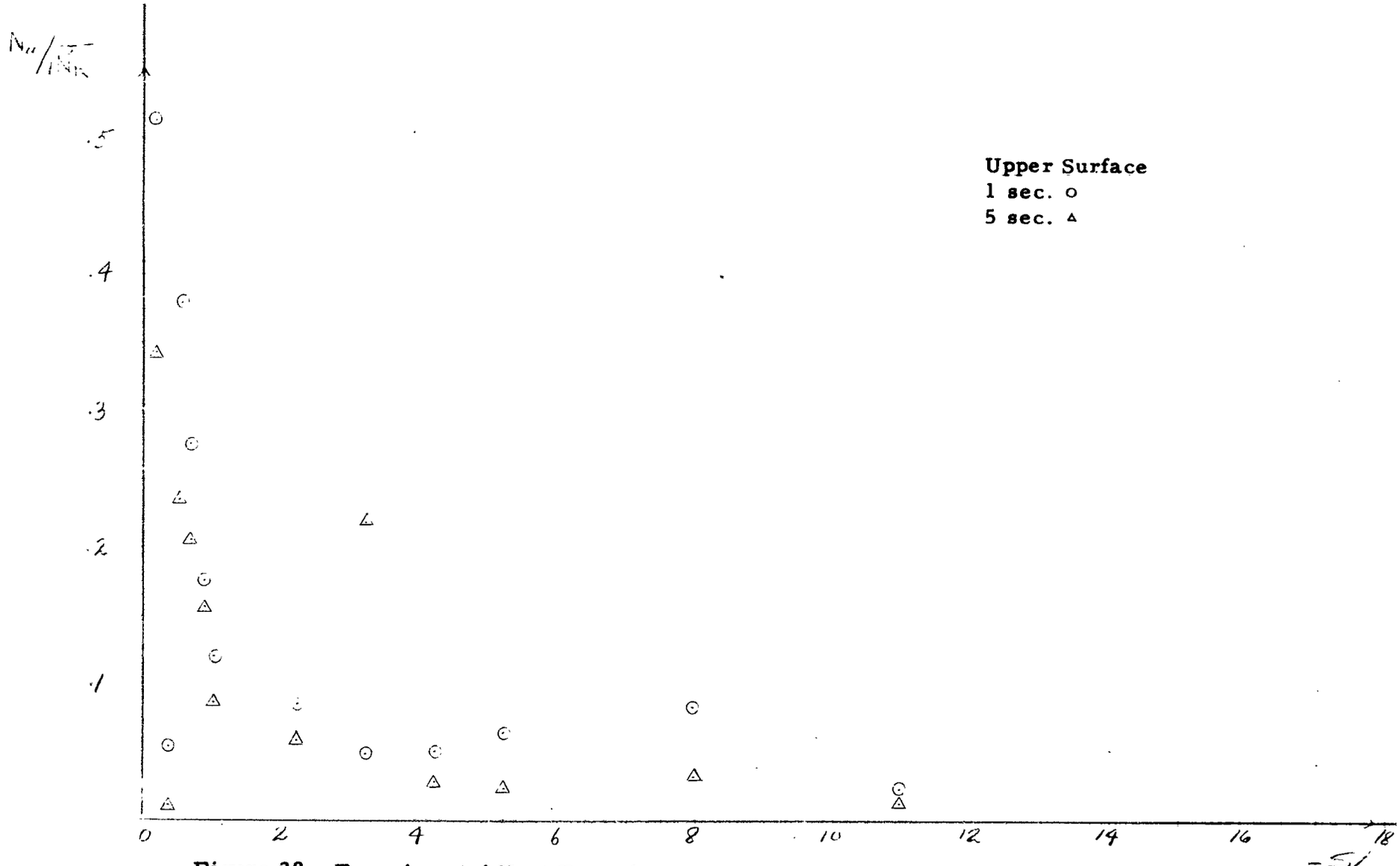

Figure 38. Experimental Heat Transfer Distribution on Two-Dimensional, Asymmetric, Blunt Body at Mach 8.08, $\alpha = 20$.

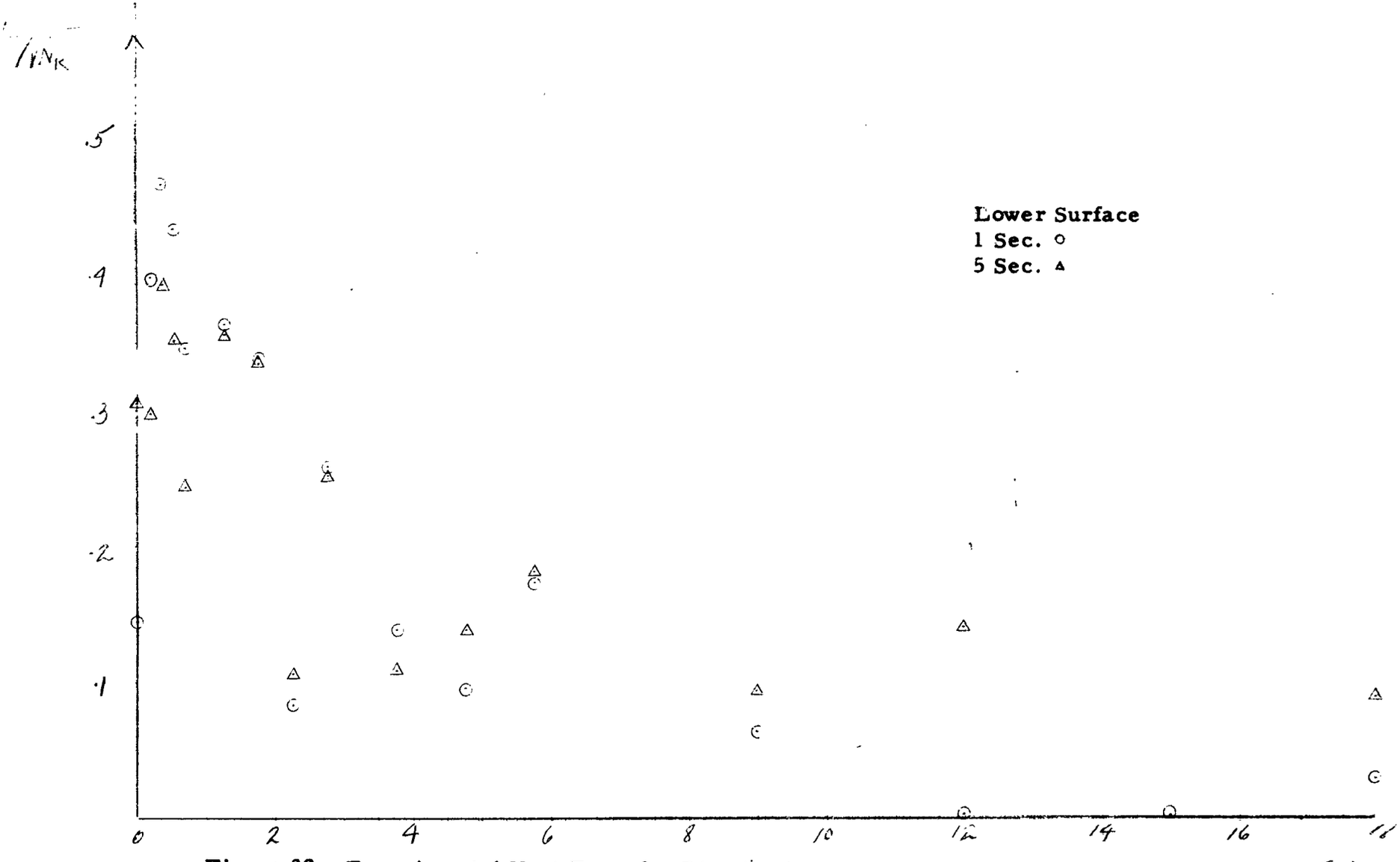

Figure 39. Experimental Heat Transfer Distribution on Two-Dimensional, Asymmetric, Blunt Body at Mach 8.08, α = 25.

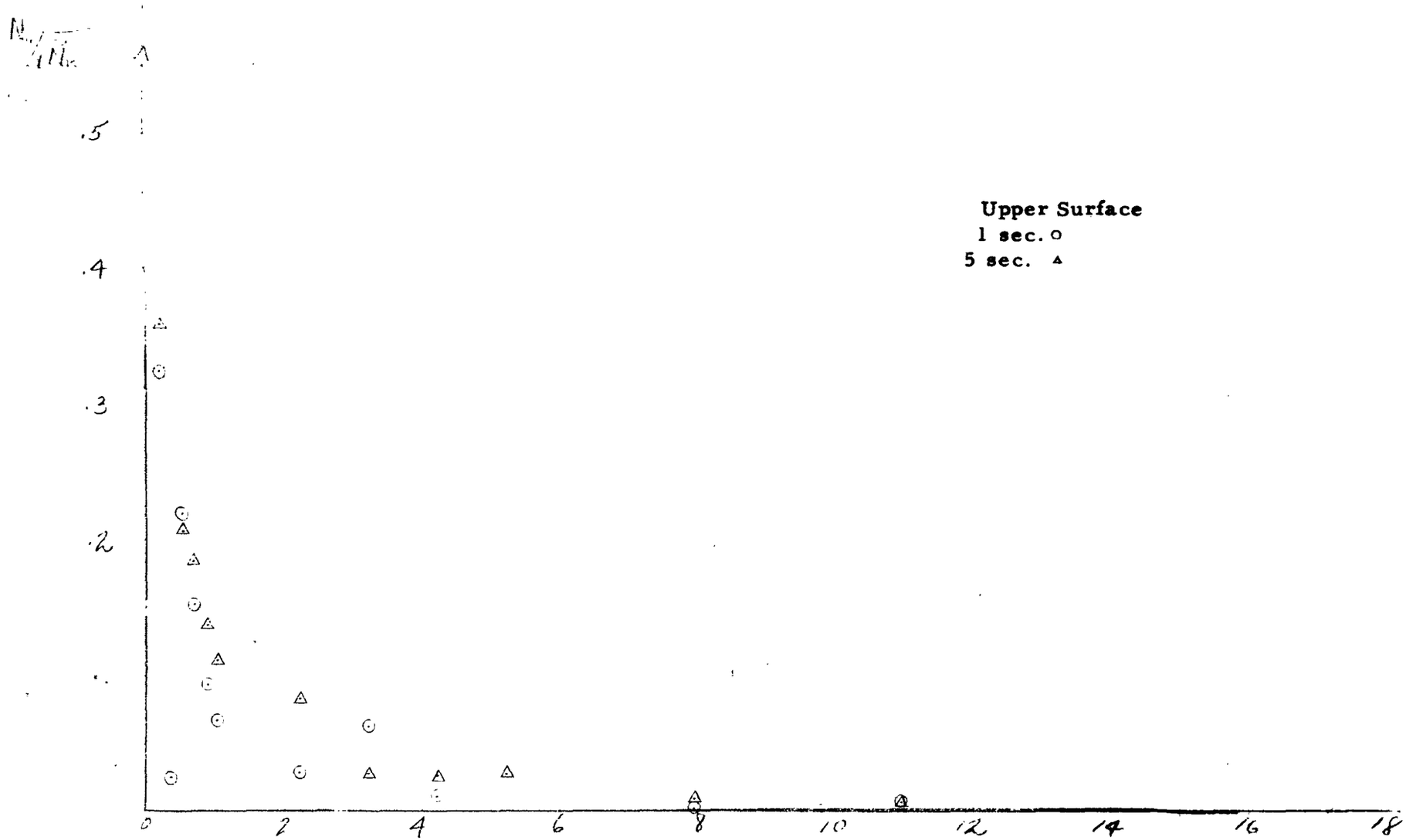

Figure 40. Experimental Heat Transfer Distribution on Two-Dimensional, Asymmetric, Blunt Body at Mach 8.08, $\alpha = 25$.